Incoherent pion photoproduction on the deuteron with polarization observables. II. Influence of final state rescattering

A. Fix and H. Arenhövel
Institut für Kernphysik, Johannes Gutenberg-Universität Mainz, D-55099 Mainz, Germany
(Received 3 June 2005; published 29 December 2005)

Incoherent pion photoproduction on the deuteron is studied for photon energies from threshold up to 1 GeV, with special emphasis on polarization observables. The elementary $\gamma N \to \pi N$ amplitude is taken from the MAID model. We investigate the influence of final state interactions on total and semi-exclusive cross sections $\vec{d}(\vec{\gamma}, \pi)NN$ by including complete rescattering in the final NN and πN subsystems. For charged-pion production the influence of NN rescattering is moderate whereas πN rescattering is almost negligible. Much stronger influences of NN rescattering are seen in neutral-pion production, which are due to the elimination of a significant spurious coherent contribution in the impulse approximation. Sizable effects are also found in some of the beam, target, and beam-target asymmetries of the differential cross section.

DOI: 10.1103/PhysRevC.72.064005 PACS number(s): 13.60.Le, 21.45.+v, 24.70.+s, 25.20.Lj

I. INTRODUCTION

Photoproduction of pions on the deuteron has two main but complementary points of interest. The first one is to obtain information on the elementary reaction on the neutron by use of the deuteron as an effective neutron target. A prerequisite for this is that one has reliable control of off-shell and medium effects. To minimize such effects, quasi-free kinematics is preferred. The second, but not secondary, aspect is just the influence of a nuclear environment on the production process, for the study of which off-quasi-free kinematics is better suited.

Pion photoproduction on the deuteron has been studied quite extensively over the past 50 years, starting with early work in Refs. [1–3]. The role of final state interaction (FSI) was investigated by Laget [4,5], who applied a diagrammatic approach. The influence of FSI effects were found to be quite small for charged-pion photoproduction compared with the neutral channel. A satisfactory agreement with experimental data was achieved for π^- production [6]. Subsequently, these results were confirmed by Levchuk *et al*. [7] for the $d(\gamma, \pi^0)np$ reaction for which the elementary photoproduction operator of Blomqvist and Laget [3] was used. This work was improved and extended to charged-pion production channels in Ref. [8], in which a more realistic elementary production operator from the SAID [9] and MAID [10] multipole analyses was taken and NN rescattering included, based on the Bonn r-space potential [11]. The influence of NN FSI was confirmed, and good agreement with experimental data was achieved. In the threshold region a sizable effect from πN rescattering was noted in Ref. [12] that arises from intermediate charged-pion production with subsequent charge-exchange rescattering on the spectator nucleon. The influence of NN and πN rescattering on polarization observables has been investigated in Ref. [7] for the Gerasimov-Drell-Hearn (GDH) sum rule in the $\pi^0 np$ channel as well as in Ref. [13] for target asymmetries in the $\pi^- pp$ reaction.

FSI effects in incoherent pion photoproduction were also studied by Darwish *et al*. [14]. The same approach was then applied to the spin asymmetry with respect to circularly polarized photons and vector-polarized deuterons [15], which determines the much-discussed GDH sum rule [16]. However, the approach was limited to the $\Delta(1232)$-resonance region in view of a relatively simple elementary production operator, based on an effective Lagrangian approach from Schmidt *et al*. [17]. A puzzling result of this work was that the influence of the FSI on the total cross sections for charged-pion production resulted in a slight decrease in the Δ-resonance region in contrast to previous work [4,5,8], in which a slight increase was found. Recently, this work was extended in a series of papers [18–22] to a study of various polarization asymmetries of the semiexclusive differential cross section for $\vec{d}(\vec{\gamma}, \pi)NN$. The semiexclusive beam asymmetry Σ for linearly polarized photons and the target asymmetries T_{IM} with respect to polarized deuterons were considered in Ref. [18] and beam-target asymmetries in [19], in both cases only in the impulse approximation (IA). FSI effects were subsequently discussed in Refs. [20–22]. Unfortunately, many of these results are based on incorrect expressions for polarization observables, as pointed out recently in Ref. [23], in which a thorough derivation of these observables is given.

Thus the present work was motivated first to use a better elementary production operator from the MAID model [10], allowing one to go to higher photon energies and also to give a more reliable description of the threshold region. Second, we would like to clarify the role of the FSI in view of the above-mentioned differences in the role of FSI effects. Third, the increasing importance of polarization observables requires a more thorough and reliable treatment as done in Refs. [18–22]. In the present work we consider again, besides the IA, complete rescattering in the final two-body subsystems, i.e., in the NN and πN subsystems. Results on the spin asymmetry of the total cross section, based on the present approach, and its contribution to the GDH sum rule have already been reported in Ref. [24].

In the next section we briefly review the basic formalism for the general differential cross section with inclusion of polarization observables as derived in Ref. [23]. Furthermore, the essential ingredients for the calculation of the T matrix in the IA and the rescattering contributions are described here. The results on the unpolarized differential cross section for the

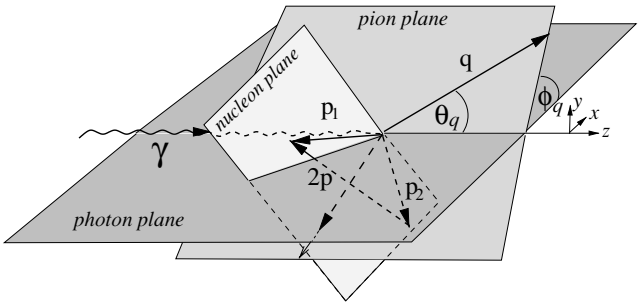

FIG. 1. Kinematics of pion photoproduction on the deuteron in the laboratory system.

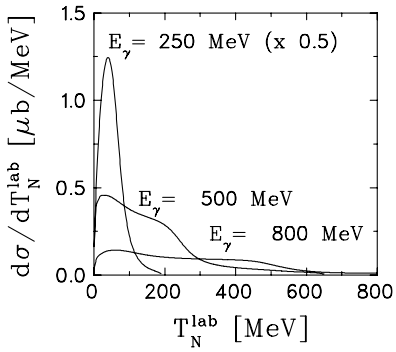

FIG. 2. Semiexclusive differential cross section $d\sigma/dT_N$ in the IA with respect to the equivalent nucleon laboratory kinetic energy T_N of NN scattering for three photon energies, $E_\gamma = 250$, 500, and 800 MeV.

semiexclusive process $\vec{d}(\vec{\gamma},\pi)NN$ as well as all beam, target, and beam-target asymmetries are presented and discussed in Sec. III together with a comparison with existing data. Finally, we conclude in Sec. IV with a summary and an outlook. The separation of the various asymmetries of the semiexclusive differential cross section are discussed in Appendix A, and a modified IA is given in Appendix B.

II. THE FORMALISM

To begin with, we briefly outline the kinematic framework of the reaction under study, namely

$$\gamma(k,\vec{\varepsilon}_\mu)+d(p_d)\rightarrow\pi(q)+N_1(p_1)+N_2(p_2), \tag{1}$$

defining the notation of the four-momenta of the participating particles. The circular polarization of the photon is denoted by $\vec{\varepsilon}_\mu$ ($\mu=\pm1$). For the description of cross sections and polarization observables we take as our reference frame the laboratory frame and as independent variables for the characterization of the final state the outgoing pion momentum $\vec{q}=(q,\theta_q,\phi_q)$ and the spherical angles $\Omega_p=(\theta_p,\phi_p)$ of the relative momentum $\vec{p}=(\vec{p}_1-\vec{p}_2)/2=(p,\Omega_p)$ of the two outgoing nucleons. The coordinate system is chosen as right handed with the z axis along the photon momentum $\vec{k}$. According to the convention of Ref. [23], we distinguish in general three planes: (i) the photon plane spanned by the photon momentum and the direction of maximal linear photon polarization, which defines the direction of the x axis; (ii) the pion plane, spanned by photon and pion momenta, which intersects the photon plane along the z axis with an angle ϕ_q; and (iii) the nucleon plane spanned by total and relative momenta of the two nucleons. It intersects the pion plane along the total momentum of the two nucleons (see Fig. 1). In case the linear photon polarization vanishes, one can choose $\phi_q=0$ and then photon and pion planes coincide.

A. The T matrix

All observables are determined by the T-matrix elements of the electromagnetic pion production current $J_{\gamma\pi}$ between the initial deuteron and the final πNN states:

$$T_{sm_s,\mu m_d}(q,\Omega_q,\Omega_p)=-^{(-)}\langle\vec{q},\vec{p};sm_s|\vec{\varepsilon}_\mu\cdot\vec{J}_{\gamma\pi}(0)|\vec{d};1m_d\rangle, \tag{2}$$

where s and m_s denote the total spin and its projection on the relative momentum of the outgoing two nucleons and m_d correspondingly denotes the deuteron spin projection on the chosen z axis. As is shown in Ref. [23], the dependence on ϕ_q can be split, i.e.,

$$T_{sm_s\mu m_d}(q,\Omega_q,\Omega_p)=e^{i(\mu+m_d-m_s)\phi_q}t_{sm_s\mu m_d}(q,\theta_q,\theta_p,\phi_{pq}). \tag{3}$$

Thus the small t matrix depends on, besides q, θ_q, and θ_p, only the difference of the azimuthal angles of $\vec{q}$ and $\vec{p}$, i.e., on $\phi_{pq}=\phi_p-\phi_q$. The small t-matrix elements are the basic quantities that determine the differential cross section and asymmetries. The latter are listed explicitly in Ref. [23].

For the calculation of the T matrix we start from the IA to which the contributions from NN and πN rescattering are added. Possible two-body contributions to the electromagnetic interaction are neglected. Thus the treatment is completely analogous to previous work on incoherent π and η photoproduction on the deuteron [14,25], to which the reader is referred for formal details. Then the T matrix is given by the sum

$$T_{sm_s\mu m_d}=T^{\rm IA}_{sm_s\mu m_d}+T^{NN}_{sm_s\mu m_d}+T^{\pi N}_{sm_s\mu m_d}. \tag{4}$$

For the IA contribution, which describes the production on one nucleon while the other acts as a spectator, one has

$$\begin{aligned}T^{\rm IA}_{sm_s\mu m_d}&=\langle\vec{q},\vec{p},\ sm_s\,|\,[t_{\gamma\pi}(1)+t_{\gamma\pi}(2)]|1\,m_d\rangle\\&=\sum_{m_s'}[\langle sm_s\,|\,\langle\vec{p}_1|t_{\gamma\pi}(W_{\gamma N_1})|-\vec{p}_2\rangle\\&\quad\times\phi_{m_s'm_d}(\vec{p}_2)|1\,m_s'\rangle-(1\leftrightarrow2)],\end{aligned} \tag{5}$$

where $t_{\gamma\pi}$ denotes the elementary pion photoproduction operator, which we take from the MAID model, $W_{\gamma N_1}$ is the invariant energy of the γN system, $\vec{p}_{1/2}=(\vec{k}-\vec{q}\,)/2\pm\vec{p}$, and $\phi_{m_sm_d}(\vec{p}\,)$ is related to the internal deuteron wave function in momentum space by

$$\begin{aligned}\langle\vec{p},1m_s|1m_d\rangle^{(d)}&=\phi_{m_sm_d}(\vec{p}\,)\\&=\sum_{L=0,2}\sum_{m_L}i^L(Lm_L1m_s|1m_d)\\&\quad\times u_L(p)Y_{Lm_L}(\hat{p}).\end{aligned} \tag{6}$$

In view of the fact that for neutral pion production the major influence of NN rescattering arises from the nonorthogonality

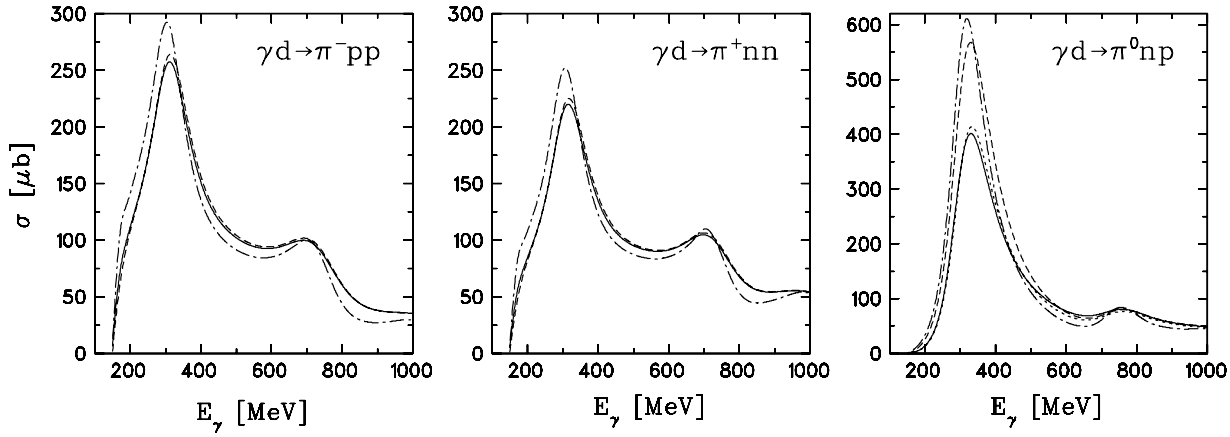

FIG. 3. Total cross section for pion photoproduction on the deuteron. Notation of curves: dashed: IA; solid, IA + *NN* and πN rescattering; dash-dotted, corresponding elementary cross section; for π^0 production, the dotted curve describes the modified IA.

of the final *NN* plane wave to the deuteron ground state, we considered in addition a modified IA amplitude, for which the deuteron component is projected out from the final plane wave (see Appendix B for details).

The two rescattering contributions have a similar structure:

$$T^{NN}_{sm_s\mu m_d} = \langle \vec{q}, \vec{p}, sm_s | t_{NN} G_{NN} [t_{\gamma\pi}(W_{\gamma N_1}) + t_{\gamma\pi}(W_{\gamma N_2})] | 1\, m_d \rangle, \quad (7)$$

$$T^{\pi N}_{sm_s\mu m_d} = \langle \vec{q}, \vec{p}, sm_s | t_{\pi N} G_{\pi N} [t_{\gamma\pi}(W_{\gamma N_1}) + t_{\gamma\pi}(W_{\gamma N_2})] | 1\, m_d \rangle, \quad (8)$$

where t_{NN} and $t_{\pi N}$ denote respectively the *NN* and πN scattering matrices and G_{NN} and $G_{\pi N}$ denote the corresponding free two-body propagators. For the actual evaluation, the scattering matrices are expanded into partial waves, and the expansion is then truncated at a certain angular momentum such that convergence is achieved.

B. The differential cross section including polarization asymmetries

The general fivefold differential cross section $d^5\sigma/dqd\Omega_q d\Omega_p$ including beam and target polarization has been derived in Ref. [23], and we refer to this work for details. In this work we are interested in the semiexclusive reaction $\vec{d}(\vec{\gamma}, \pi)NN$ in which only the produced pion is detected. This means integration of the fivefold differential cross section over Ω_p, yielding as the semiexclusive differential cross section [23]

$$\frac{d^3\sigma}{dqd\Omega_q} = \frac{d^3\sigma_0}{dqd\Omega_q}\Bigg(1 + P_l^\gamma \Bigg\{\widetilde{\Sigma}^l \cos 2\phi_q + \sum_{I=1}^{2} P_I^d \times \sum_{M=-I}^{I} \widetilde{T}^l_{\rm IM} \cos[M\phi_{qd} - 2\phi_q - \delta_{I1}\pi/2] d^I_{M0}(\theta_d)\Bigg\} + \sum_{I=1}^{2} P_I^d \sum_{M=0}^{I} \big(\widetilde{T}^0_{\rm IM} \cos[M\phi_{qd} - \delta_{I1}\pi/2] + P_c^\gamma \widetilde{T}^c_{\rm IM} \sin[M\phi_{qd} + \delta_{I1}\pi/2]\big)\, d^I_{M0}(\theta_d)\Bigg), \quad (9)$$

where $\phi_{qd} = \phi_q - \phi_d$. Explicit expressions for the asymmetries $\widetilde{\Sigma}^l$, $\widetilde{T}_{\rm IM}$, and $\widetilde{T}^{c/l}_{\rm IM}$ are listed in the appendix of Ref. [23]. Furthermore, the photon polarization is characterized by the degree of circular polarization P_c^γ and the degree of linear polarization P_l^γ, where the x axis has been chosen in the direction of maximum linear polarization. The deuteron target is characterized by four parameters, namely the vector- and tensor-polarization parameters P_1^d and P_2^d, respectively, and by the orientation angles θ_d and ϕ_d of the deuteron orientation axis with respect to which the deuteron density matrix has been assumed to be diagonal.

We would like to point out that in forward and backward pion emission the following asymmetries vanish at

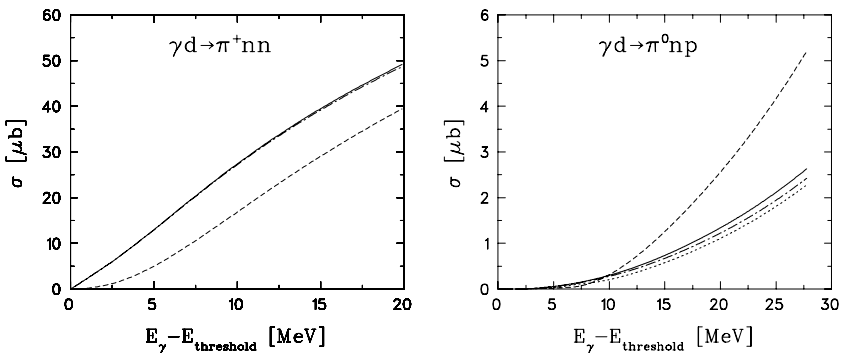

FIG. 4. Total cross section near threshold for π^+ and π^0 photoproduction on the deuteron. Notation of curves: dashed, IA; dash-dotted, IA + *NN* rescattering; solid, IA + *NN* and πN rescattering; dotted in the right-hand panel, modified IA.

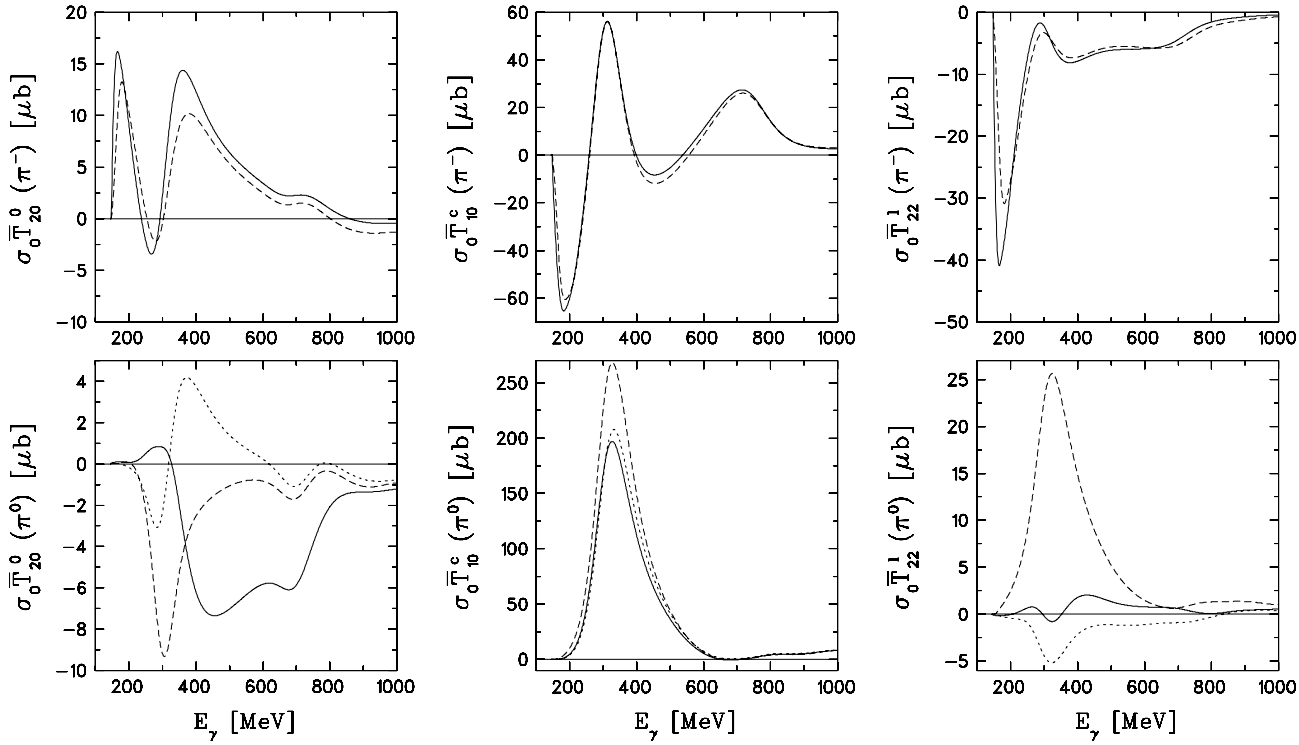

FIG. 5. Polarization asymmetries $\sigma_0 \overline{T}^0_{20}, \sigma_0 \overline{T}^c_{10}$, and $\sigma_0 \overline{T}^l_{22}$ of the total cross section for π^- (upper panels) and π^0 photoproduction (lower panels) on the deuteron. Notation of curves: dashed, IA; solid, IA + *NN* rescattering; for π^0 production, dotted curve describes the modified IA.

$\theta_q = 0$ or π:

$$\widetilde{\Sigma}^l = 0, \quad \widetilde{T}^{0,c}_{\mathrm{IM}} = 0 \text{ for } M \neq 0, \quad \text{and} \quad T^l_{\mathrm{IM}} = 0 \text{ for } M \neq 2, \tag{10}$$

because of helicity conservation, i.e., in this case the cross section should not depend on ϕ_q.

In the next section we present results for the case in which only the direction of the outgoing pion is measured, not its momentum. Then the corresponding differential cross

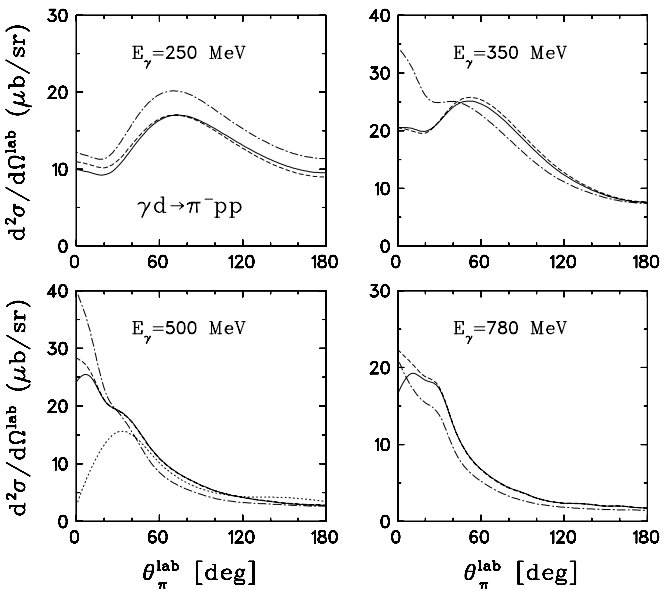

FIG. 6. Semiexclusive differential cross section for π^- photoproduction on the deuteron. Notation of curves: dashed, IA; solid, IA + *NN* rescattering; dash-dotted elementary process $n(\gamma, \pi^-)p$; dotted in lower left-hand panel, IA from [8].

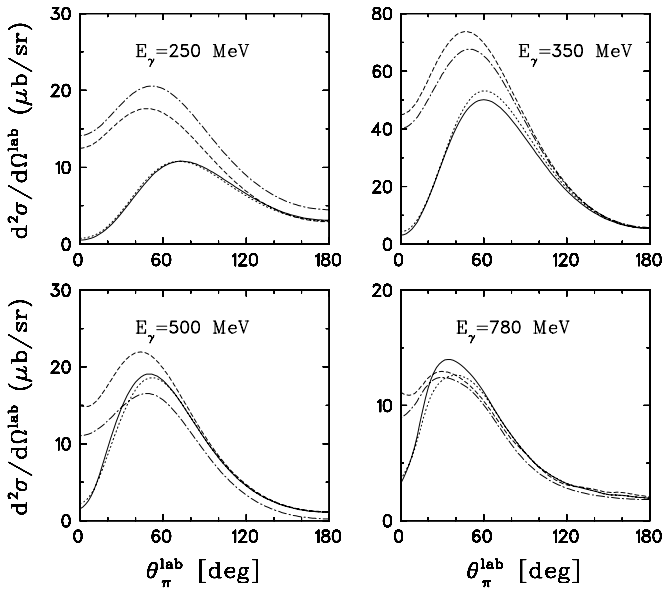

FIG. 7. Semiexclusive differential cross section for π^0 photoproduction on the deuteron. Notation of curves: dashed, IA; dotted, modified IA; solid, IA + *NN* rescattering; dash-dotted, average elementary process on neutron and proton.

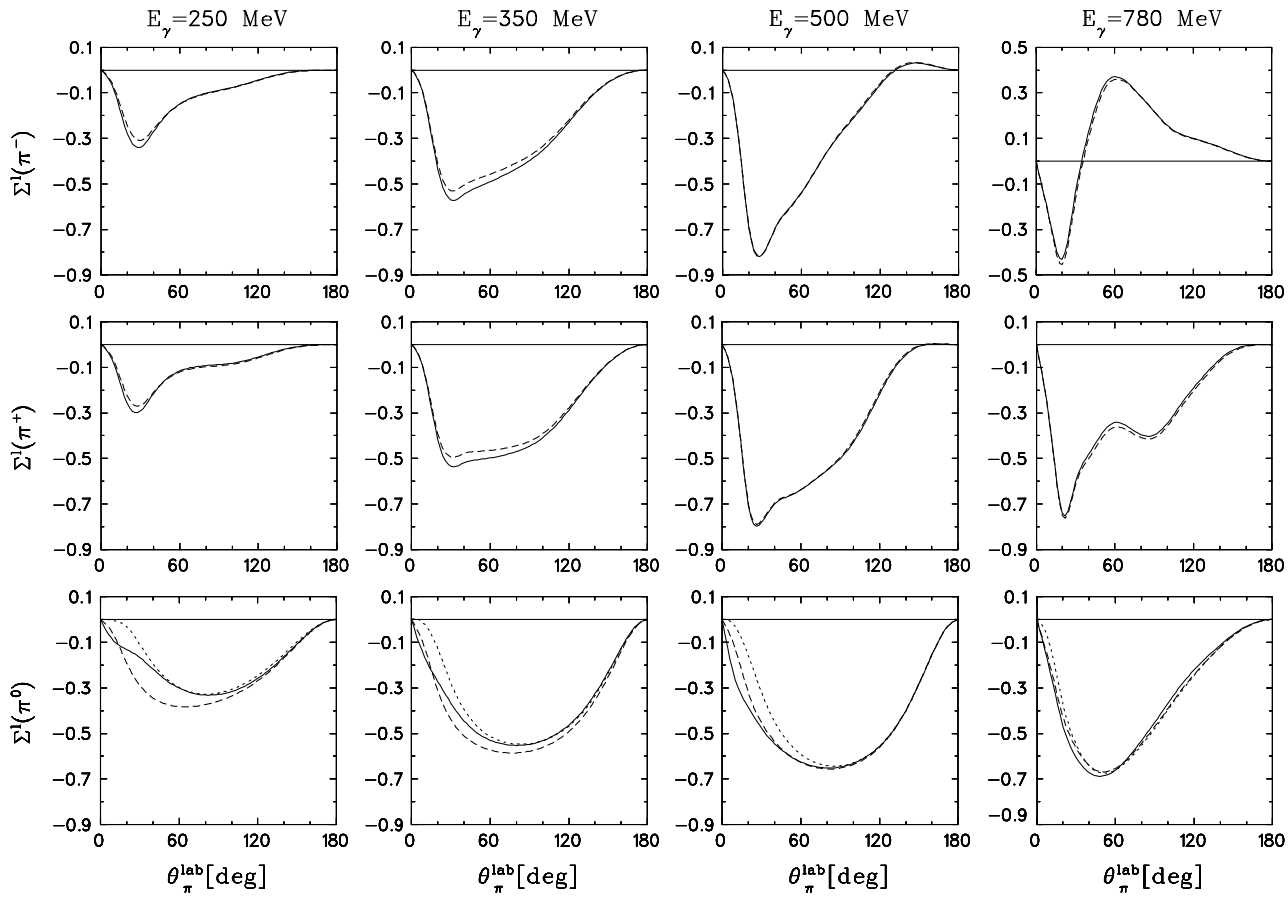

FIG. 8. Photon asymmetry Σ^l for the three charge states of semiexclusive single-pion photoproduction on the deuteron. Notation of curves: dashed, IA; dotted, modified IA for π^0 production; solid, IA + *NN* rescattering.

section $d^2\sigma/d\Omega_q$ is given by an expression formally analogous to Eq. (9), in which the unpolarized cross section and asymmetries are replaced with

$$\frac{d^3\sigma_0}{dq d\Omega_q} \to \frac{d^2\sigma_0}{d\Omega_q} = \int_{q_{\min}(\theta_q)}^{q_{\max}(\theta_q)} dq\, \frac{d^3\sigma_0}{dq d\Omega_q}, \tag{11}$$

$$\frac{d^3\sigma_0}{dq d\Omega_q}\, \widetilde{\Sigma}^l(q,\theta_q) \to \frac{d^2\sigma_0}{d\Omega_q}\, \Sigma^l(\theta_q) = \int_{q_{\min}(\theta_q)}^{q_{\max}(\theta_q)} dq\, \frac{d^3\sigma_0}{dq d\Omega_q}\, \widetilde{\Sigma}^l(q,\theta_q), \tag{12}$$

$$\frac{d^3\sigma_0}{dq d\Omega_q}\, \widetilde{T}^\alpha_{\rm IM}(q,\theta_q) \to \frac{d^2\sigma_0}{d\Omega_q}\, T^\alpha_{\rm IM}(\theta_q) = \int_{q_{\min}(\theta_q)}^{q_{\max}(\theta_q)} dq\, \frac{d^3\sigma_0}{dq d\Omega_q} \times \widetilde{T}^\alpha_{\rm IM}(q,\theta_q), \quad \alpha \in \{0,l,c\}. \tag{13}$$

The upper and lower integration limits are given by

$$q_{\max}(\theta_q) = \frac{1}{2b}\left(a\,\omega\cos\theta_q + E_{\gamma d}\sqrt{a^2 - 4b\,m_\pi^2}\right), \tag{14}$$

$$q_{\min}(\theta_q) = \max\left\{0,\, \frac{1}{2b}\left(a\,\omega\cos\theta_q - E_{\gamma d}\sqrt{a^2 - 4b\,m_\pi^2}\right)\right\}, \tag{15}$$

where

$$a = W_{\gamma d}^2 + m_\pi^2 - 4\,m_N^2, \tag{16}$$

$$b = W_{\gamma d}^2 + \omega^2 \sin^2\theta_q, \tag{17}$$

$$W_{\gamma d}^2 = m_d(m_d + 2\,\omega), \tag{18}$$

$$E_{\gamma d} = m_d + \omega. \tag{19}$$

Finally, in the total cross section only a few polarization observables survive, namely, one has [23]

$$\sigma\left(P_l^\gamma, P_c^\gamma, P_1^d, P_2^d\right) = \sigma_0\left[1 + P_2^d\,\overline{T}^0_{20}\,\frac{1}{2}(3\cos^2\theta_d - 1) + P_c^\gamma\, P_1^d\,\overline{T}^c_{10}\cos\theta_d + P_l^\gamma\, P_2^d\,\overline{T}^l_{22} \times \cos(2\phi_d)\,\frac{\sqrt{6}}{4}\sin^2\theta_d\right], \tag{20}$$

where the unpolarized total cross section and asymmetries are given by

$$\sigma_0 = \int d\Omega_q \int_{q_{\min}(\theta_q)}^{q_{\max}(\theta_q)} dq\, \frac{d^3\sigma_0}{dq d\Omega_q}, \tag{21}$$

$$\sigma_0\,\overline{T}^\alpha_{\rm IM} = \int d\Omega_q \int_{q_{\min}(\theta_q)}^{q_{\max}(\theta_q)} dq\, \frac{d^3\sigma_0}{dq d\Omega_q}\, \widetilde{T}^\alpha_{\rm IM}, \tag{22}$$

with $\alpha \in \{0,l,c\}$. This concludes the formal part.

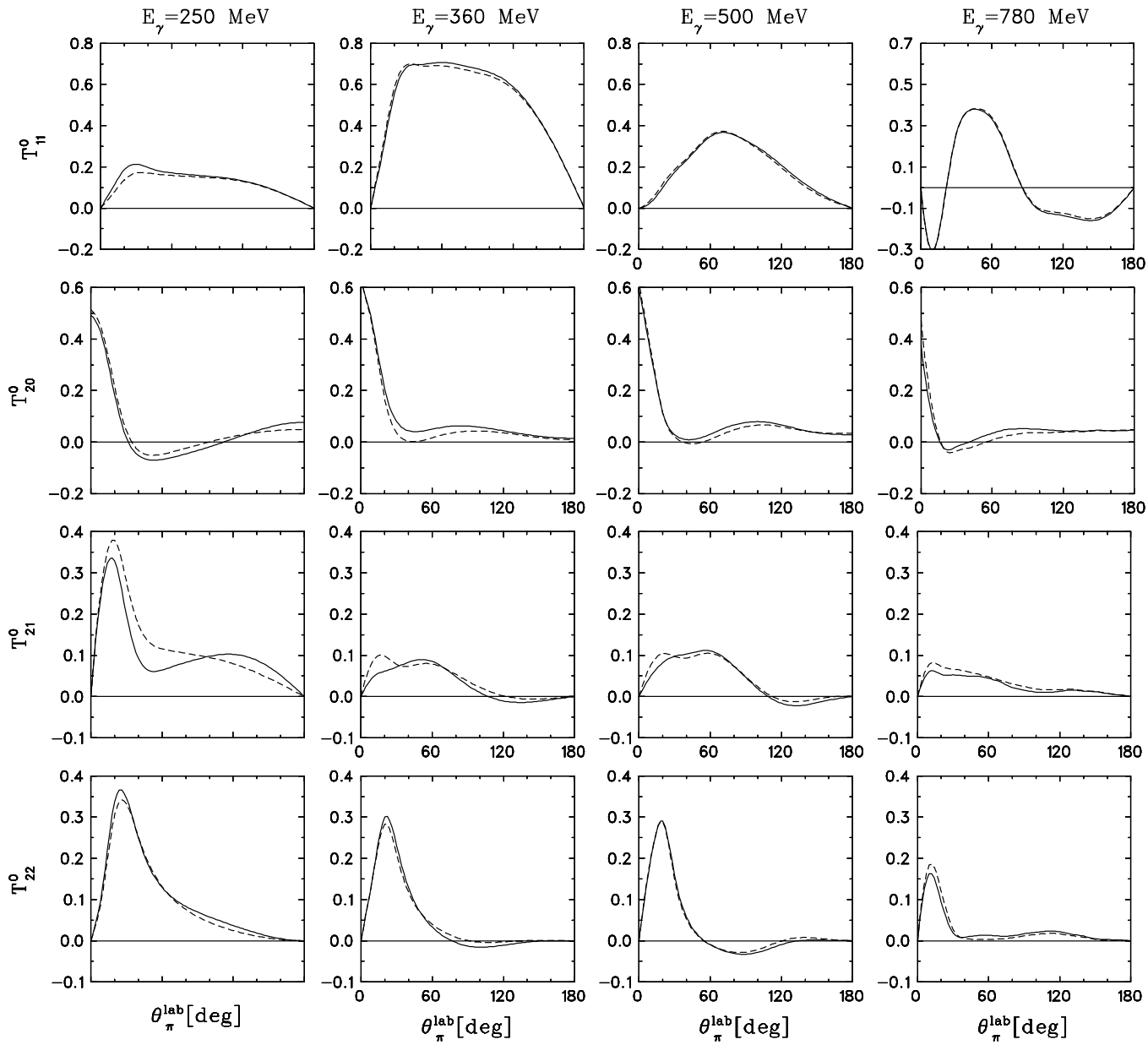

FIG. 9. Target asymmetries $T^0_{\rm IM}$ for semiexclusive π^- photoproduction on the deuteron. Notation of curves the same as in Fig. 8.

III. RESULTS AND DISCUSSION

For the calculation of the *NN*-rescattering contribution we have taken the separable representation of the realistic Paris potential from Ref. [26] and included all partial waves up to $^3D_3$. The deuteron wave function was also calculated with this potential. In principle, any other realistic potential, e.g., the Bonn r-space potential [11], could be used as well, because the results do not depend sensitively on the potential model, as was found in Ref. [14]. However, one comment is in order with respect to the question of whether the use of such a nonrelativistic *NN* potential can be justified in view of the high energies involved, because the potential is fit to *NN*-scattering data up to nucleon laboratory kinetic energies of $T_{NN} = 330$ MeV only. However, even up to $T_{NN} = 500$ MeV, it reproduces the phase shifts reasonably well because the inelasticity parameters are still small. Since the calculation of *NN* rescattering requires *NN*-scattering amplitudes also at considerably higher energies, for which we still use the same separable representation, we might expect some serious error. On the other hand, the size of this error depends on the relative size of that part of the phase space at which the energy of the *NN* subsystem exceeds the region of validity. To estimate the corresponding error, we present in Fig. 2 the cross section $d\sigma/dT_N$ as a function of the equivalent nucleon kinetic lab energy T_N of *NN* scattering. One readily notes that even for a photon energy of 800 MeV the dominant part of the cross section corresponds to nucleon laboratory kinetic energies of less than 500 MeV. Thus the use of such a realistic potential is justified.

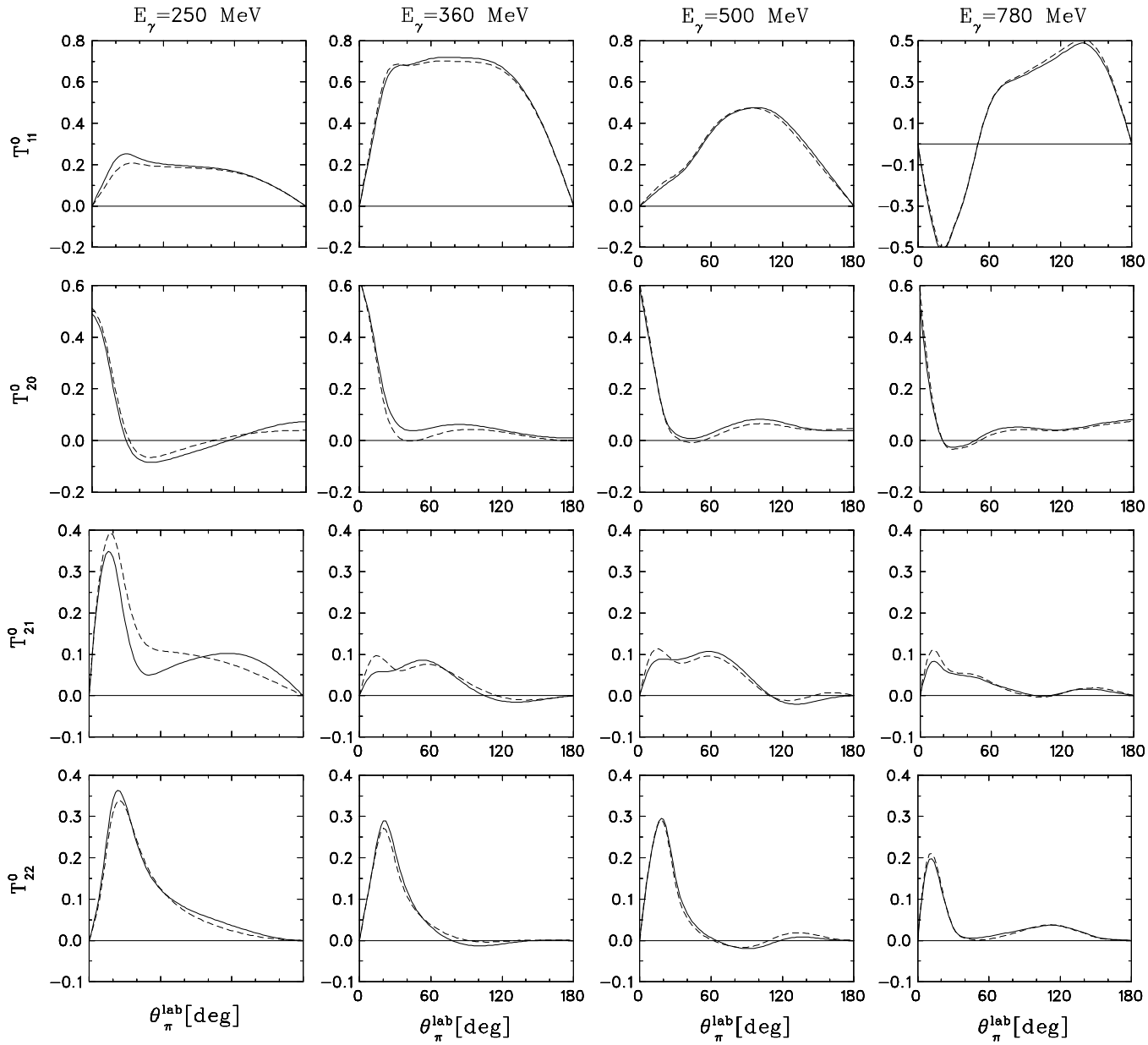

FIG. 10. Target asymmetries $T^0_{\rm IM}$ for semiexclusive π^+ photoproduction on the deuteron. Notation of curves the same as the in Fig. 8.

Similarly, πN rescattering is evaluated by use of a realistic separable representation of the πN interaction from Ref. [27] and with all partial waves up to $l = 2$ taken into account. We have evaluated the semiexclusive differential cross section, including the various polarization asymmetries in the IA alone and with the inclusion of NN and πN rescattering. As already mentioned, the elementary pion photoproduction amplitude is taken from the MAID2003 model as parametrized in terms of invariant amplitudes defined in Ref. [28]. For this purpose we assume on-shell conditions for the pion and the active nucleon in the final state. Then we determine the initial four-momentum p_i of the active nucleon by assuming four-momentum conservation at the elementary vertex, i.e., $p_i = q + p_f - k$.

A. Total cross sections

We begin the discussion of the results with the total cross sections for the three charge states displayed in Fig. 3, where we have plotted in addition the corresponding elementary cross section for comparison. The threshold region is separately plotted in Fig. 4.

One readily notes that for charged-pion production the rescattering effects are in general quite small. Only when close to threshold do they lead to a sizable enhancement (see left-hand panel of Fig. 4), mainly by NN rescattering, while πN rescattering is almost negligible.

The significant role of the NN FSI in photoproduction of mesons at very low energies has been noted previously in Refs. [5,25,29,30]. We mention here only that this effect has a

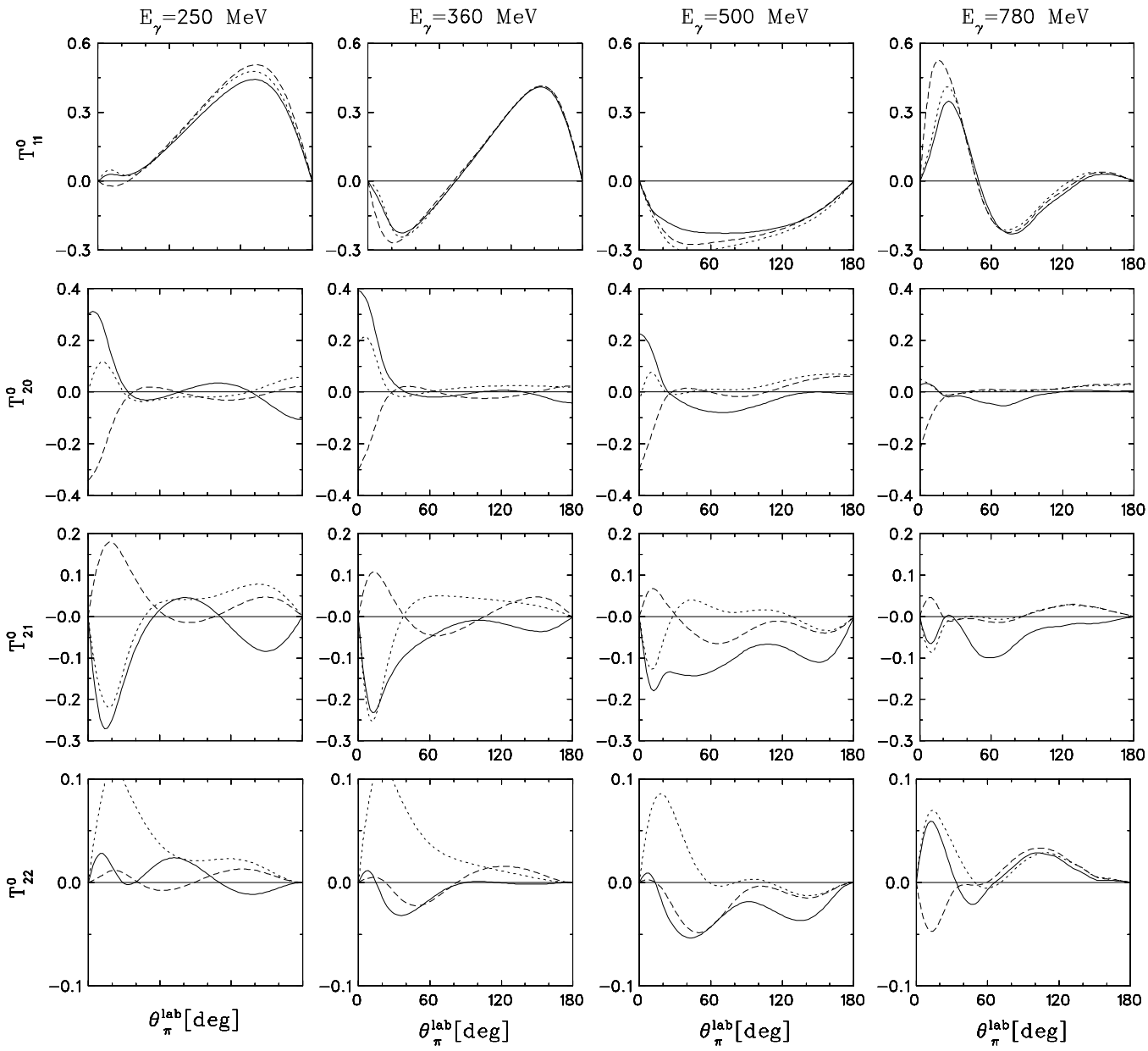

FIG. 11. Target asymmetries $T^0_{\rm IM}$ for semiexclusive π^0 photoproduction on the deuteron. Notation of curves the same as in Fig. 8.

kinematical rather than a dynamical origin. As pointed out in Ref. [25], in the IA the energy needed for pion production below the free nucleon threshold is provided exclusively through the high momentum of a nucleon moving toward the incoming photon. As a result, the IA predicts an anomalous suppression of the cross section, because of a small probability of finding a nucleon with high momentum in the deuteron wave function. Thus *NN* rescattering provides a mechanism to balance the strong mismatch between the momentum needed to produce the pion and the characteristic internal nucleon momentum in the deuteron, so that the strong suppression appearing in IA can be avoided. The same reasoning is true for the π^0 channel. However, in this case the subsequently mentioned role of orthogonality turns out to be very important, so that the resulting FSI effect becomes destructive already at 10 MeV and higher above threshold.

At higher energies, near and above the maximum, the cross sections of charged-pion production are reduced by the FSI by a few percent. Therefore the main difference to the elementary cross section comes from the Fermi motion, leading to a slight reduction and a shift of the maximum, and a broadening of the whole distribution. As one can see in Fig. 3, the result of these features is that the energy-integrated cross section,

$$I(E) = \int_{E_{\rm th}}^{E} \sigma(E_\gamma) dE_\gamma, \tag{23}$$

as a function of the upper integration limit E, is preserved over a wide energy region. In other words, the integral at $E = 1$ GeV

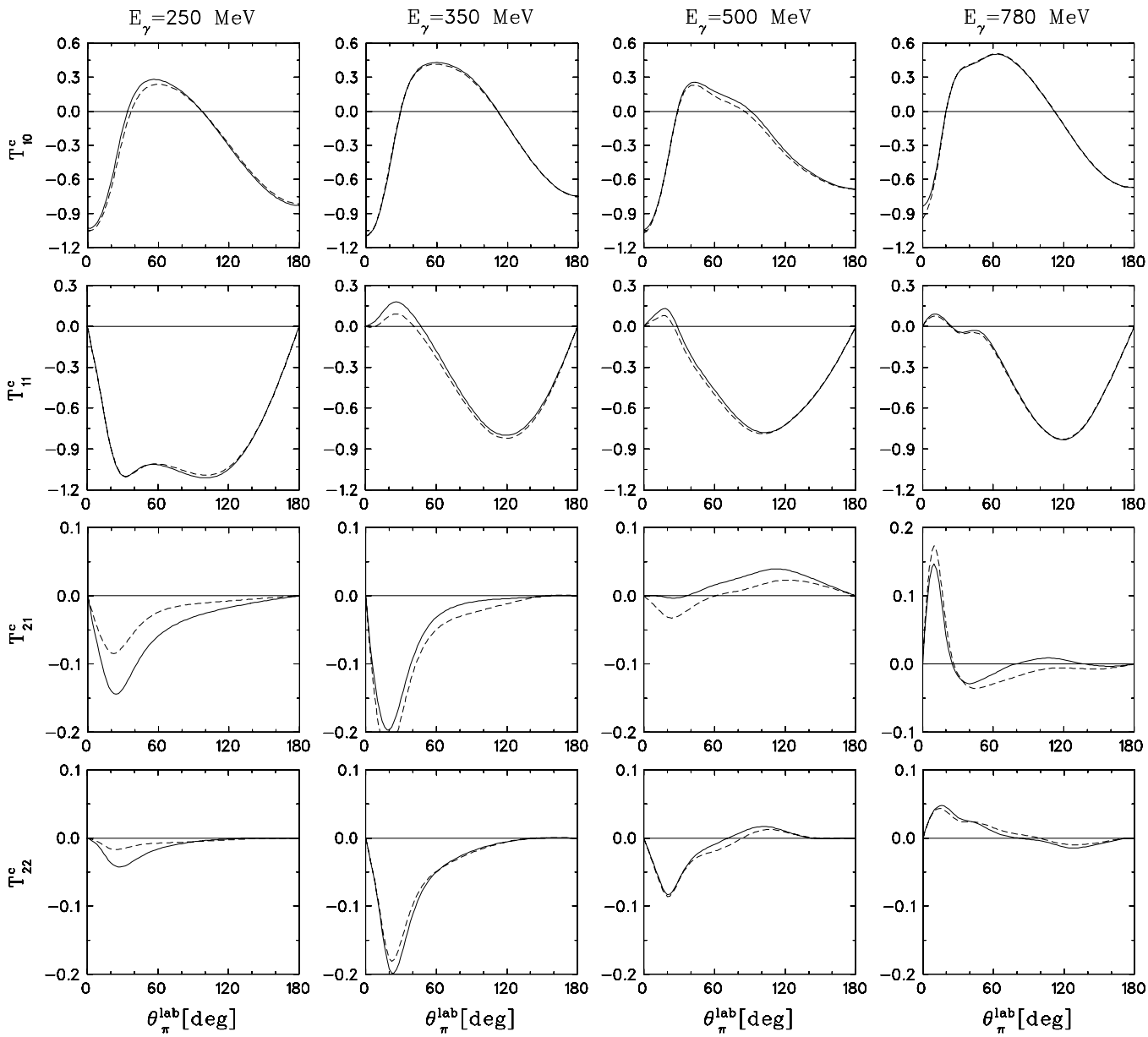

FIG. 12. Beam-target asymmetries $T^c_{\rm IM}$ for circularly polarized photons and polarized deuterons for semiexclusive π^- photoproduction on the deuteron. Notation of curves the same as in Fig. 8.

has approximately the same value for the reaction on the free nucleon and on the deuteron. Concerning the role of the FSI in the $\pi^\pm$ channels at higher energies, one can assume that the interaction between the emitted particles leads basically to a redistribution of events in phase space, so that in the absence of absorption the overall yield of particles does not change and the FSI effect in the total cross section remains insignificant. It is, however, not the case for the near-threshold region where, as discussed above, the IA amplitude turns out to be anomalously suppressed in the available phase space.

One notes quite large FSI effects, in contrast to charged-pion production, from *NN* rescattering in π^0 production, as displayed in the right-hand panel of Fig. 3. However, these effects are mainly due to the elimination of the spurious coherent contribution in the IA. That is nicely demonstrated by the results for the modified IA, also shown in Fig. 3, where the deuteron wave-function component in the final plane wave is projected out (see Appendix B for details). The additional rescattering contributions beyond the orthogonality effect are comparable with what was found in charged-pion production, except near threshold, where one finds a much smaller influence of the FSI. With respect to the elementary cross section, one notes a sizable reduction for incoherent π^0 production on the deuteron, because part of the strength goes to the coherent channel $d(\gamma, \pi^0)d$. The spurious admixture of the coherent channel in the IA cross section was also discussed in Ref. [31].

The polarization observables of the total cross section are shown in Fig. 5 only for π^- and π^0 production since the ones for π^+ and π^- production are quite similar. The vector

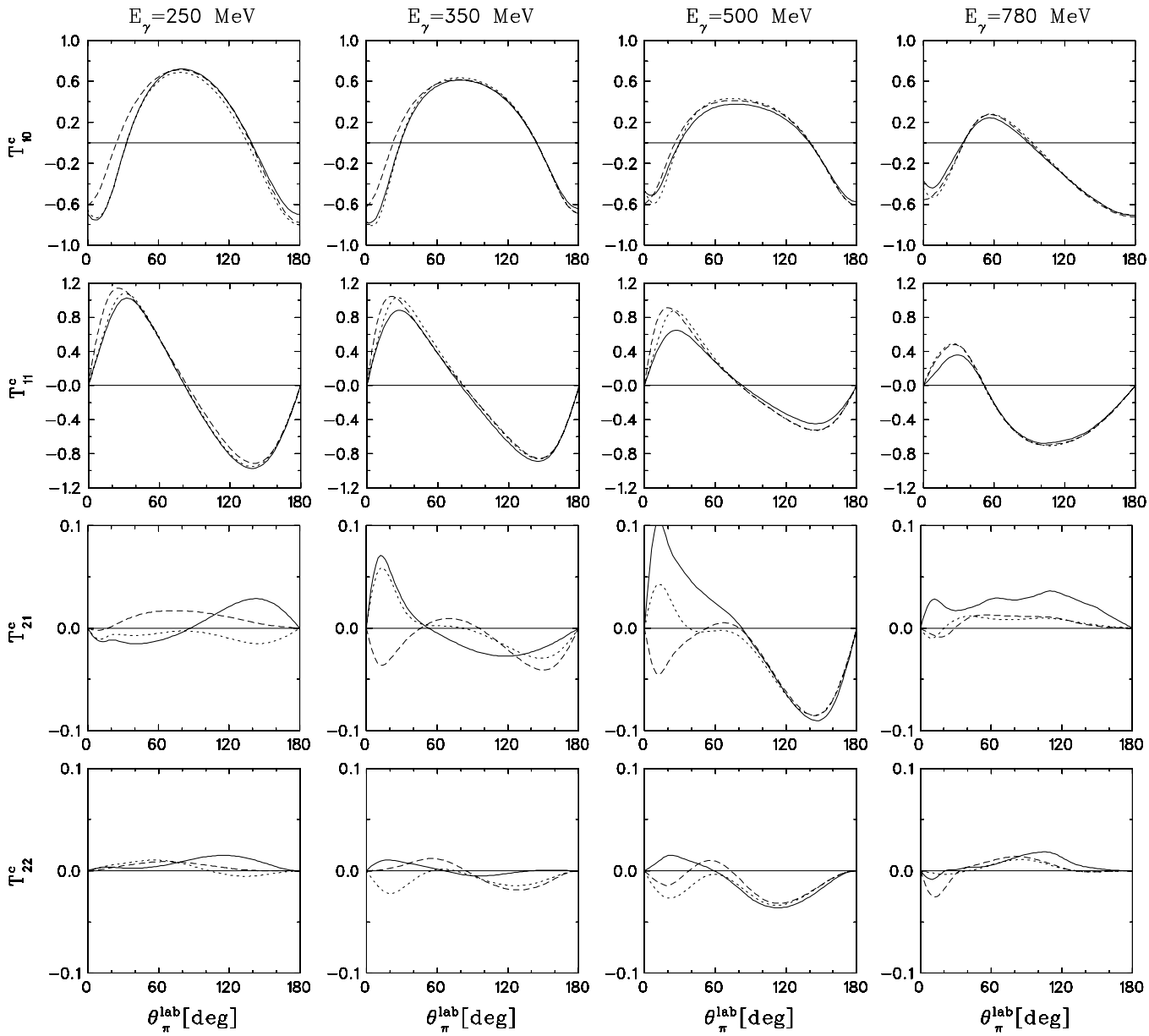

FIG. 13. Beam-target asymmetries $T^c_{\rm IM}$ for circularly polarized photons and polarized deuterons for semiexclusive π^0 photoproduction on the deuteron. Notation of curves the same as in Fig. 8.

asymmetry for circularly polarized photons $\sigma_0 \overline{T}^{\,c}_{10}$ (middle panels), which governs the spin asymmetry of the GDH sum rule, reproduces the results reported in Ref. [24]. The sensitivity to the FSI is weak, similar to the total cross sections. The tensor asymmetries for π^- production are sizable in the near-threshold region, exhibiting a sharp peak in absolute values. $\sigma_0 \overline{T}^{\,0}_{20}$ reaches a second, quite broad maximum above the Δ resonance, while $\sigma_0 \overline{T}^{\,l}_{22}$ remains small. The FSI is more notable than in the total cross section. For π^0 production, the tensor asymmetries show quite a different behavior compared with that of π^- production. They are quite small in general, almost vanishing in the near-threshold region. Furthermore, they show huge FSI effects beyond the orthogonality effect.

B. Differential cross section

Angular distributions are shown in Fig. 6 for π^- production and in Fig. 7 for π^0 production. As for the total cross section, one notes for π^- production a small size of rescattering effects. At the lowest energy (250 MeV) they decrease the cross section at forward angles and increase it in the backward direction. At 350 MeV one finds a slight enhancement near the maximum, while at the two higher energies a sizable decrease is found only in the extreme forward direction. For comparison, we show also the elementary cross sections, and again the smoothing effect of the Fermi motion is apparent.

Comparing our calculation with the predictions of Refs. [5] and [8] we note a significant disagreement for the IA at forward angles. At $E_\gamma = 500$ MeV our IA cross section

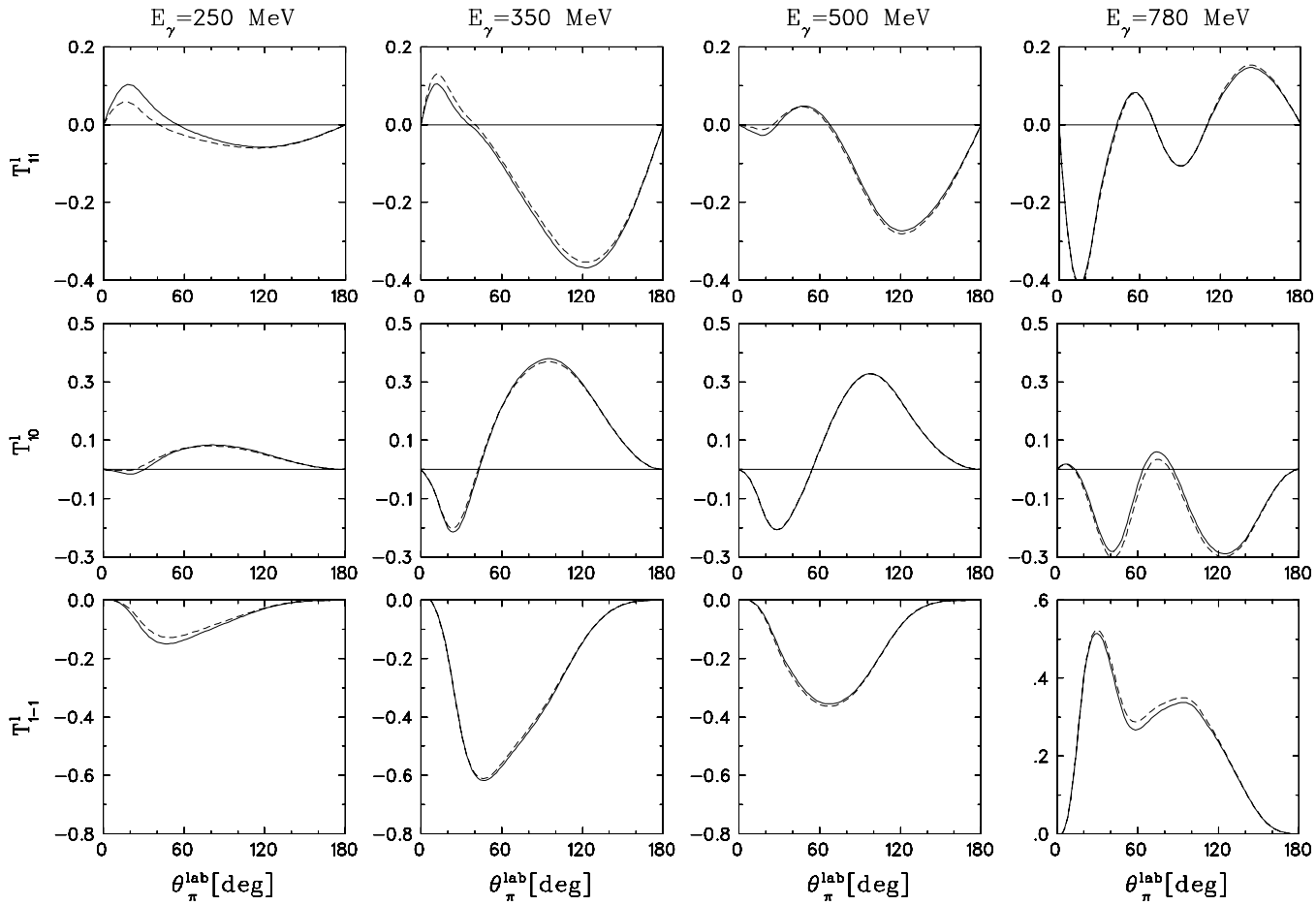

FIG. 14. Beam-target asymmetries T^l_{1M} for linearly polarized photons and vector polarized deuterons for semiexclusive π^- photoproduction on the deuteron. Notation of curves the same as in Fig. 8.

exhibits a visible rise that is governed mainly by the pion photoelectric term in the elementary amplitude. At the same time the calculations of Ref. [8] (see dotted curve in the lower left-hand panel of Fig. 6 at $E_\gamma = 500$ MeV) predict a strong reduction in the same angular region, so that the corresponding IA result at $\theta_\pi = 0$ is about 10 times smaller than ours.

A possible reason of this discrepancy has been discussed in Ref. [14]. Namely, it was claimed in Ref. [8] that the drastic reduction of the cross section compared with the elementary reaction is a manifestation of the Pauli principle, leading to a strong suppression of the *pp* states in the region of small relative momenta in this subsystem. On the contrary, we would like to note that this suppression takes place only in the triplet state ($s = 1$) of the emitted protons, whereas the singlet part ($s = 0$), in which the processes on the individual nucleons can coherently enhance each other, peaks at $\theta_\pi = 0$, similar with the elementary cross section. The resulting angular distribution shows some reduction at forward angles, compared with the elementary reaction, which, however, is not as large as that exhibited by the triplet part only and is therefore much smaller compared with the prediction of Refs. [5,8].

On the other hand, inclusion of the FSI leads in Refs. [5,8] to a significant increase at small angles compared with the IA cross section, whereas in our case the effect of FSI is small and destructive. It is therefore interesting to note that the difference between the full results of the present work (see Fig. 24 in Subsec. III.G) and of Ref. [8] is rather small, so that both models describe the data equally well.

As was mentioned above, in the π^0 channel the orthogonality effect appears so that the role of the FSI is approximately determined by the fraction of the coherent reaction $\gamma d \to \pi^0 d$ in the inclusive π^0 photoproduction. Figure 7 demonstrates the huge spurious contribution of the coherent process in the IA that is eliminated when the modified IA is applied. This result could be expected because the effect of orthogonality should be especially visible in the region of small pion angles, where the momentum transferred to the nucleons is minimal and the overlap between initial and final wave functions is most important. The additional FSI effects are quite small. It is only at 350 MeV that one notes a slight increase of the cross section near the maximum around 60° and at 780 MeV a more sizable increase.

C. Beam asymmetry for linearly polarized photons

Next we turn to the beam asymmetry Σ^l displayed in Fig. 8 for the three charge states at various energies in the

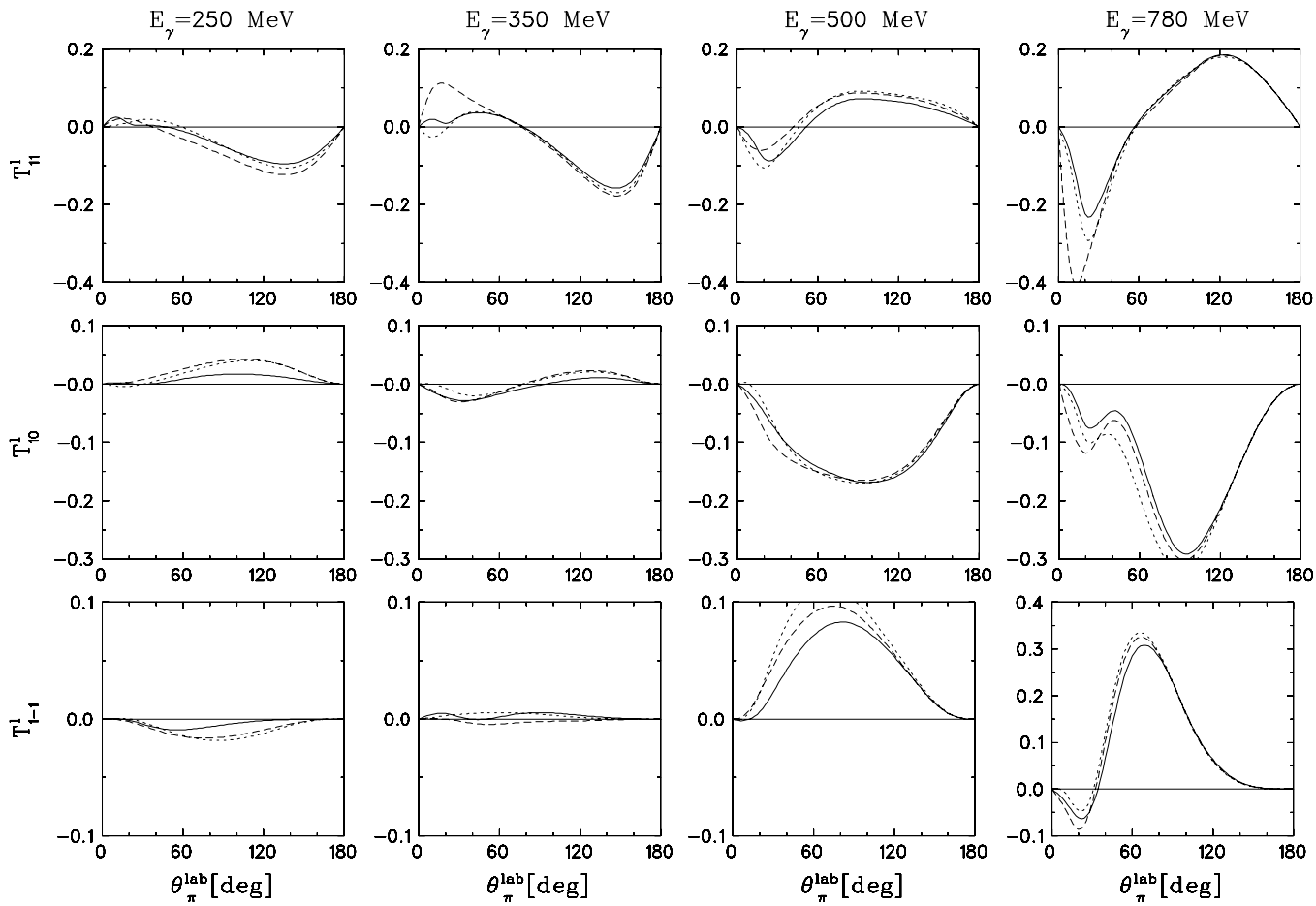

FIG. 15. Beam-target asymmetries T^l_{1M}-for linearly polarized photons and vector-polarized deuterons for semiexclusive π^0 photoproduction on the deuteron. Notation of curves the same as in Fig. 8.

Δ-resonance region and above. In all of these asymmetries one notes a relatively small influence from the FSI. We consider first the results for π^- production in the top panels of Fig. 8. For the lowest three energies the photon asymmetry Σ^l is negative. It is quite small below the Δ region and increases considerably in absolute size with increasing energy, becoming quite broad around 350 Mev but more forward peaked at 500 Mev. At the highest energy of 780 MeV one notes a different behavior. The deep minimum in the forward direction turns into a broad positive distribution above 40°. The three lowest energies are also representative for π^+ production (middle panels of Fig. 8). However, at the highest energy the asymmetry remains negative, but exhibits a secondary minimum around 90°.

The Σ^l asymmetry for π^0 production, shown in the lowest panels of Fig. 8, exhibits quite a different behavior compared with that of charged-pion production. One finds a broad, structureless, and sinus-shaped negative distribution with a maximum around 80°–90° with increasing amplitude by about a factor of 2 going from 250 to 500 MeV. At 780 MeV the width of the distribution becomes smaller and the minimum moves toward forward angles. In general also here the influence of rescattering is small. It is mainly due to the removal of the spurious coherent contribution. The relatively largest influence appears at the lowest energy of $E_\gamma = 250$ MeV.

Compared with the results in Refs. [18,19,21], here one readily notes quite substantial differences for both charged- and neutral-pion production, both in angular behavior and also in absolute size, in particular at higher energies. For π^- production a larger influence of the FSI is found in Ref. [22] that we cannot confirm. Furthermore, Σ^l does not vanish in Ref. [22] at $\theta_q = 0$ and π as it should, although it is small. Strangely enough, the authors mention this feature as a notable effect. The origin of these differences is not clear. In any case, the comparison suffers from the questionable formal expressions used for the calculation of Σ^l that, moreover, differ in the various publications [18,21,22].

D. Target asymmetries for oriented deuteron

The target asymmetries T^0_{1M} are shown in Figs. 9–11 for the three charge states, respectively. In view of the similarity of the asymmetries for the two charge states, except for T^0_{11} at 780 MeV, we restrict the discussion to π^- and π^0 production. In general FSI effects are again small; the largest appear in T^0_{21}. The vector asymmetry T^0_{11} is positive up to 500 MeV and shows a broad distribution over the whole angular range. However, at 780 MeV an oscillatory behavior develops with sizable amplitude. It is only at the lowest energy of

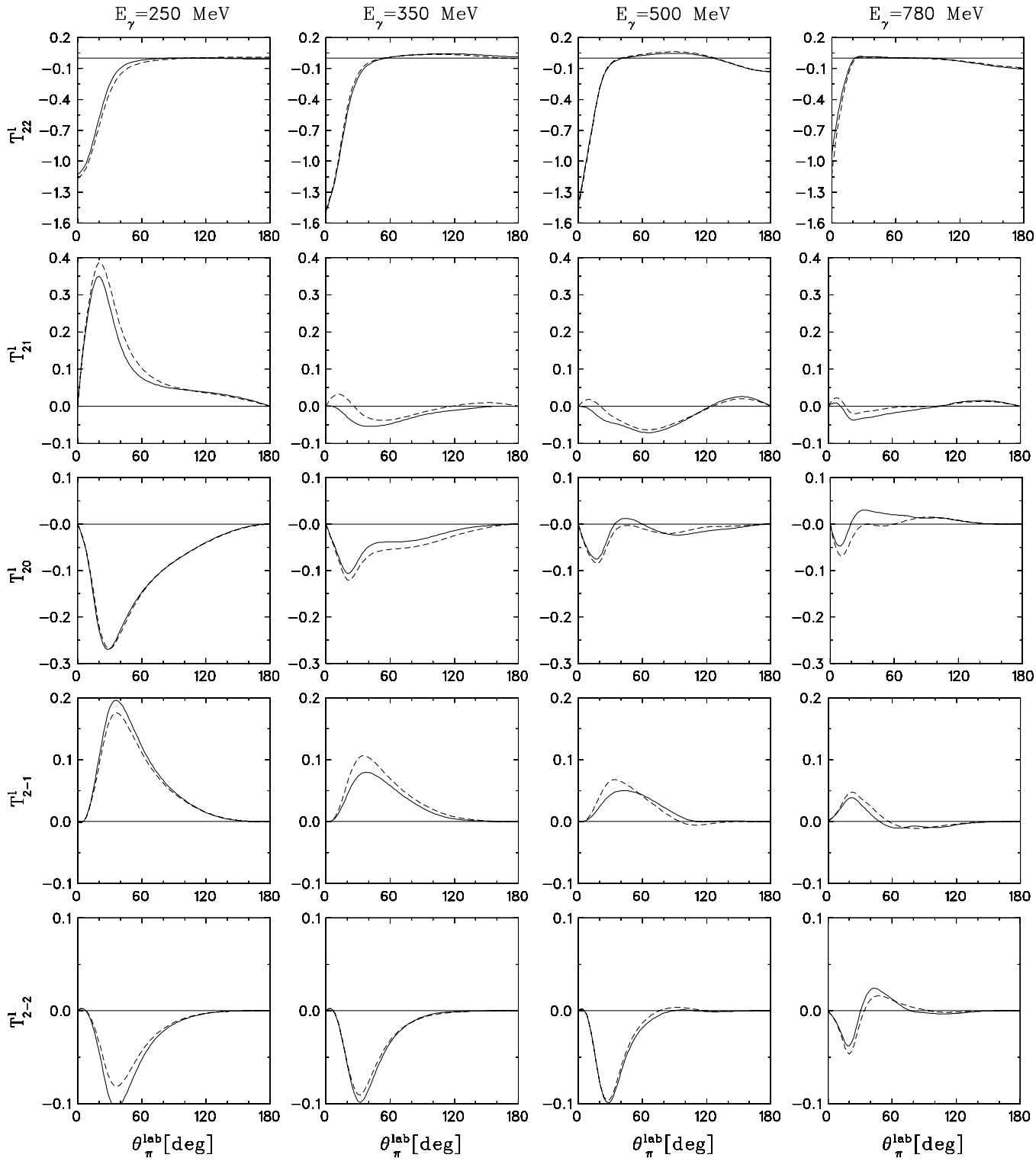

FIG. 16. Beam-target asymmetries T^l_{2M} for linearly polarized photons and tensor-polarized deuterons for semiexclusive π^- photoproduction on the deuteron. Notation of curves the same as in Fig. 8.

$E_\gamma = 250$ MeV that one notes some notable influence at forward angles from the FSI. With respect to Refs. [18,19,22] we find an opposite sign, a smaller amplitude, and also a somewhat different angular behavior.

The tensor target asymmetry T^0_{20} exhibits a pronounced sharp peak at 0° and a rapid falloff with increasing angles, remaining quite small above 30°. The results are similar to those of Refs. [18,19,22] except that, in contrast to the

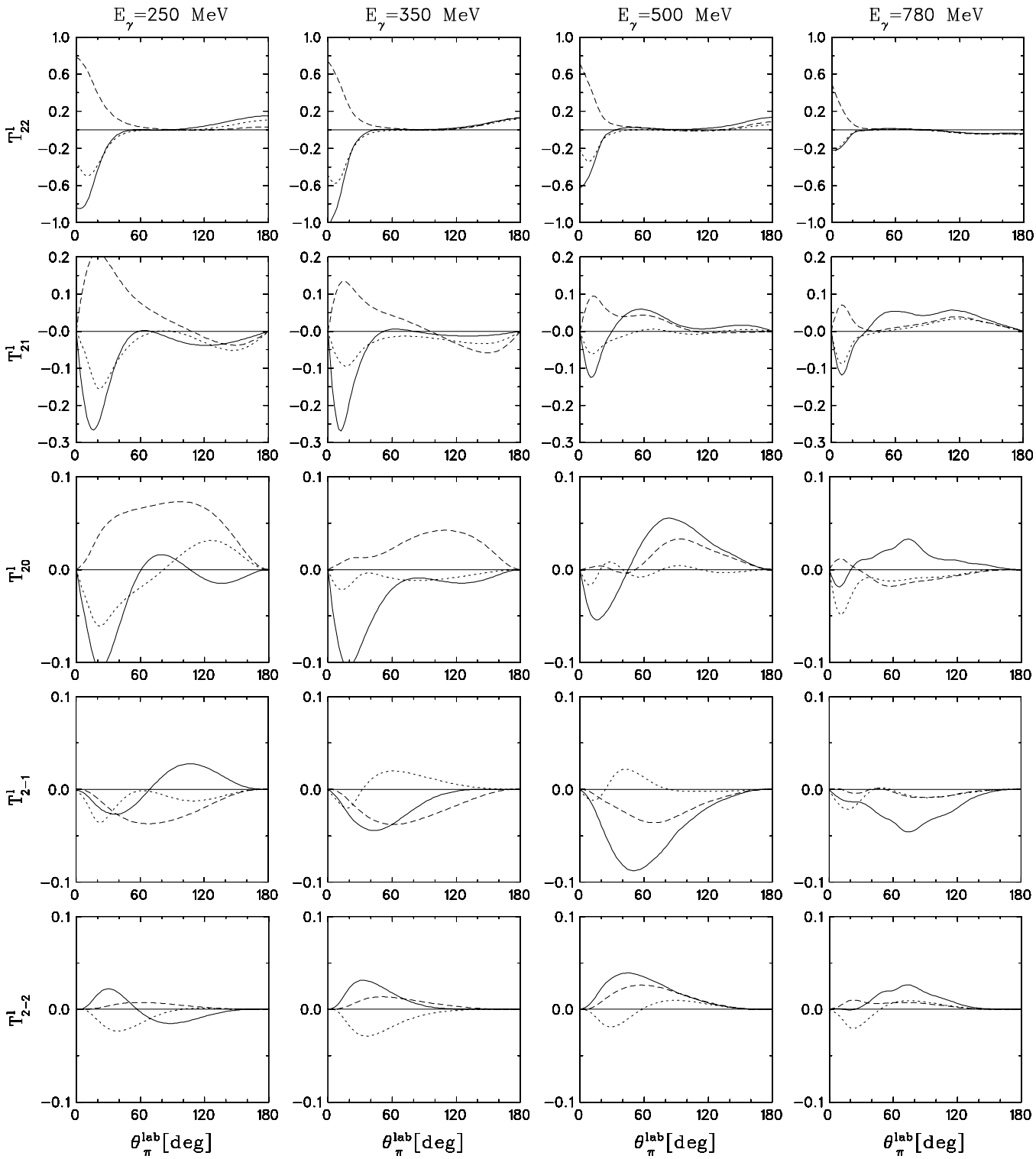

FIG. 17. Beam-target asymmetries T^l_{2M} for linearly polarized photons and tensor-polarized deuterons for semiexclusive π^0 photoproduction on the deuteron. Notation of curves the same as in Fig. 8.

small negative values of Refs. [18,19] at backward angles, we find small positive values. Moreover, we find smaller FSI influences at backward angles than those in Ref. [22]. T^0_{21} peaks at small angles around 20° for $E_\gamma = 250$ MeV, which disappears at the three higher energies, becoming a broader distribution with a considerably smaller size. The FSI shows some notable influence. Again we find significant differences from Refs. [18,19] with respect to shape, size, and FSI effects, in particular at the lowest energy. Finally, T^0_{22} exhibits a prominent peak in the forward direction that becomes sharper

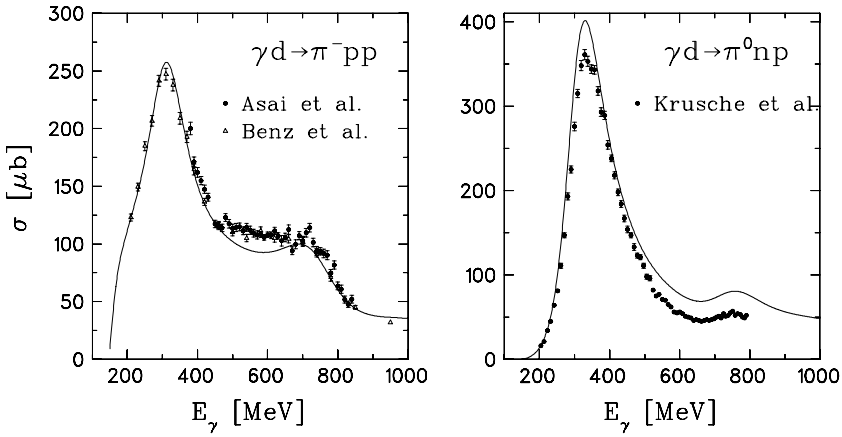

FIG. 18. Total cross section for π^- (left-hand panel) and π^0 photoproduction (right-hand panel) on the deuteron. Solid curves: IA + *NN* and πN rescattering. Experimental data from Benz *et al*. [6] and from Asai *et al*. [32] for π^- production and from Krusche *et al*. [33] for π^0 production.

and moves toward smaller angles with increasing photon energy. This is in qualitative agreement with Refs. [18,19], although the size is different and our FSI effects are much smaller.

The target asymmetries for π^0 production in Fig. 11 show quite a different behavior compared with that of charged-pion production. The structure of T_{11}^0 changes significantly with energy. While at $E_\gamma = 250$ MeV one finds a maximum around 130°, one notes a forward negative minimum and a backward positive maximum at $E_\gamma = 350$ MeV, at $E_\gamma = 500$ MeV a broad and quite flat negative distribution, and finally at 780 MeV a forward maximum and a negative minimum around 80°. The tensor asymmetries are much more sensitive to the FSI. This is particularly apparent in T_{20}^0 exhibiting a forward negative minimum in the IA that turns into a positive forward peak when the FSI is switched on. Also T_{21}^0 shows such a drastic influence from the FSI. T_{22}^0 is much smaller than for charged-pion production and shows an oscillatory behavior. FSI effects are noticeable again. For these asymmetries the differences from the results of Refs. [18,19] are again quite significant.

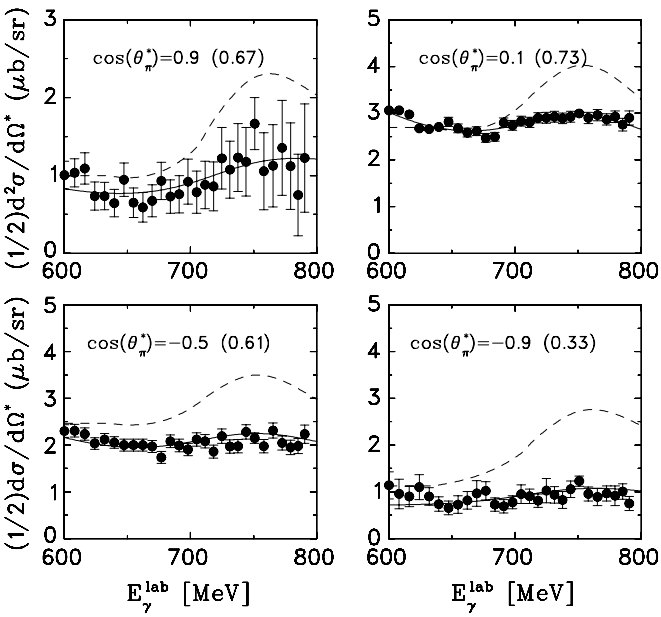

FIG. 19. Differential cross section for π^0 production on the deuteron as a function of the lab photon energy for fixed pion angles in the equivalent γN c.m. system. The cross section is plotted per nucleon. Notation of curves: solid, full calculation multiplied by the factors in parentheses; dashed, MAID prediction for the sum $1/2[d\sigma(\pi^0 p) + d\sigma(\pi^0 n)]$.

E. Beam-target asymmetries for circularly polarized photons

Next we discuss the double-polarization asymmetries $T_{\rm IM}^c$ for circularly polarized photons and oriented deuterons. They are in a certain sense complementary to the target asymmetries $T_{\rm IM}^0$ because, while one is the real part, the other is the imaginary part of the basic quantities $V_{\rm IM}^1$ as defined in Ref. [23]. Since the results for the two charged pions are again in general quite similar, we display the results only for π^- in Fig. 12 and for π^0 in Fig. 13. In contrast to what has been claimed in Ref. [19], all of them are nonvanishing. As a side remark, although T_{10}^c should vanish according to Ref. [19], a nonvanishing spin asymmetry is reported in Ref. [20]. For both π^0 and π^-, the vector asymmetry T_{10}^c is quite sizable in the forward and backward directions and also around 90° for π^0. It is this asymmetry that determines the GDH sum rule. The

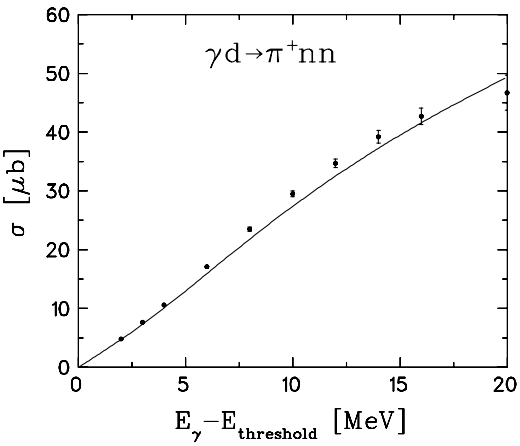

FIG. 20. Total cross section near threshold for π^+ photoproduction on the deuteron. Solid curve, IA + *NN* and πN rescattering. Experimental data from Booth *et al*. [35].

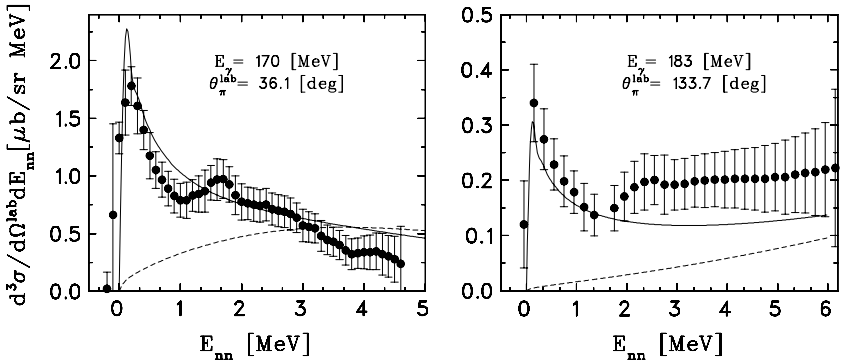

FIG. 21. Semiexclusive differential cross section $d^3\sigma/d\Omega_\pi\, dE_{nn}$ for π^+ photoproduction on the deuteron at a fixed pion angle as a function of the relative energy E_{nn} of the final two neutrons. Solid curves, IA + *NN* rescattering. Experimental data from Köbschall *et al*. [37].

influence of the FSI is quite marginal, in particular for π^-. For both charge states the energy dependence is weak. The other vector asymmetry, T_{11}^c, shows a rather different behavior. For π^- it is predominantly negative with a slight preference of the backward direction, especially at higher energies, while for π^0 it has a positive maximum around 30° and a negative minimum around 150°, almost independent of the energy. Considerably smaller are the tensor asymmetries T_{21}^c and T_{22}^c, but they are a little more sensitive to the FSI. This is particularly apparent for T_{21}^c in π^0 production above the Δ-resonance region.

F. Beam-target asymmetries for linearly polarized photons

The beam-target asymmetries $T_{\rm IM}^l$ for linearly polarized photons and polarized deuterons for π^- and π^0 production are shown in Figs. 14–17. These asymmetries are also very similar for the two charge states π^- and π^+. The vector asymmetries T_{1M}^l do not vanish at all, as claimed in Ref. [18]. They are small for π^- at the lowest energy of $E_\gamma = 250$ MeV, but become sizable for the higher energies (see Fig. 14). They are considerably smaller for π^0 production, as shown in Fig. 15, but more sensitive to the FSI. Of the corresponding tensor asymmetries in Figs. 16 and 17, T_{22}^l is by far the largest for both charge states π^- and π^0, exhibiting a pronounced forward peak that becomes slightly sharper with increasing energy. The size decreases significantly when going from T_{22}^l to T_{2-2}^l. By the way, they are certainly not equal, as claimed in Ref. [18]. While T_{2-2}^l is restricted to vanish at $\theta_q = 0$ and π, this is not the case for T_{22}^l. For π^- production one notes some the FSI effects in $T_{2\pm1}^l$, whereas for π^0 quite drastic influences from the FSI can be seen, leading even to a sign change in some of them. A comparison to the results in Ref. [18] makes no sense because of the above-mentioned wrong formal expressions in Ref. [18].

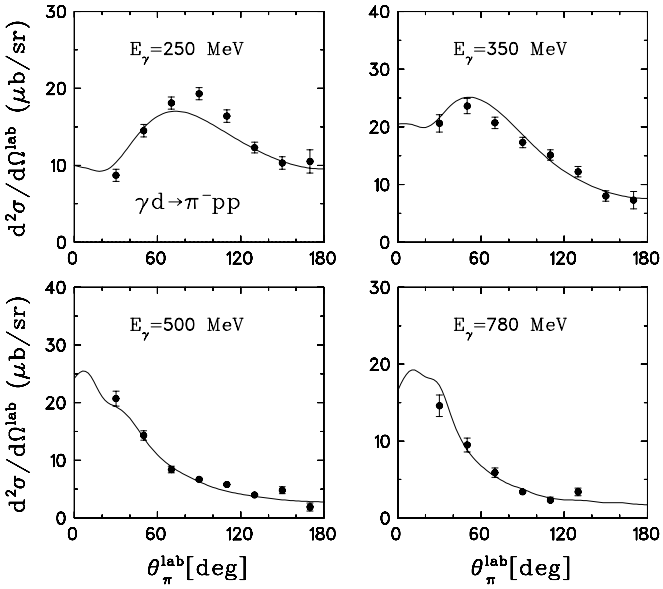

FIG. 22. Semiexclusive differential cross section for π^- photoproduction on the deuteron. Solid curves, IA + *NN* rescattering. Experimental data from Benz *et al*. [6].

G. Comparison with experiment

We now turn to a comparison with experimental data, where available. Figure 18 shows the total cross sections for π^- and π^0 production. The agreement with experimental data

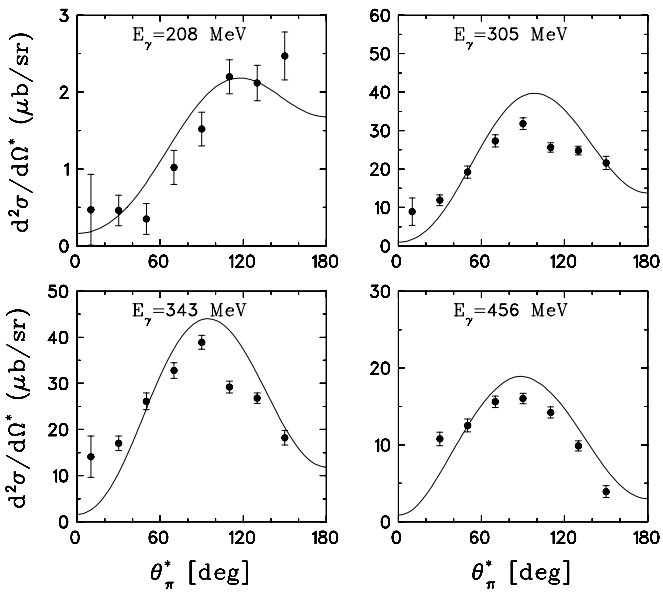

FIG. 23. Semiexclusive differential cross section for π^0 photoproduction on the deuteron. Cross section and the pion angle θ_π^* refer to the equivalent γN c.m. system of the corresponding reaction on the nucleon. Solid curves, IA + *NN* rescattering. Experimental data from Krusche *et al*. [33].

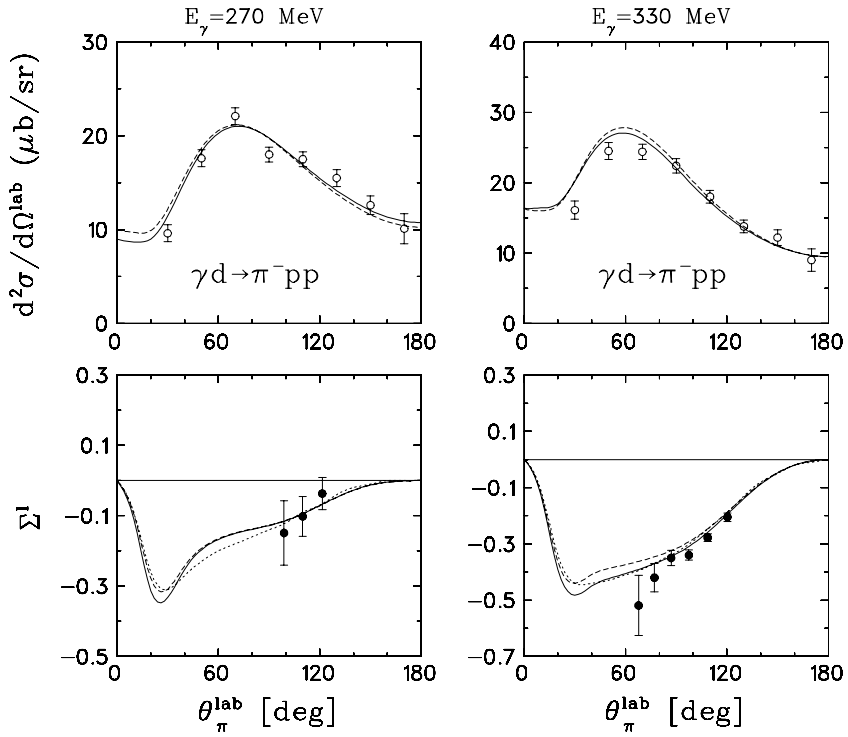

FIG. 24. Differential cross section and linear photon polarization asymmetry for semiexclusive π^- photoproduction on the deuteron. Notation of curves: dashed, IA; dotted, IA from Lee and Sato [40]; solid, IA + *NN* rescattering. The data are for the differential cross section from Benz *et al*. [6] and for the linear photon asymmetry from the LEGS Collaboration (LEGS-exp.L3b) [39].

for π^- production is satisfactory, although not perfect. The theory is a little high in the maximum but low in the dip region between the Δ and the second resonance region. For π^0, one notes some slight overshooting in the maximum and a sizable overestimation above the Δ in the second resonance region. This discrepancy was already discussed in Ref. [33], where it was noted that the smearing and damping of the second resonance peak can hardly be explained by the Fermi motion effect alone. According to our results, the broadening of the resonance structure in pion production on the deuteron is quite significant. This effect is readily seen in Fig. 19, where we present differential cross sections for π^0 production on the deuteron as functions of the photon energy for a fixed pion angle. The cross section refers to the equivalent γN c.m. system, where the nucleon is at rest in the deuteron. The solid curves are our full calculation multiplied by energy-independent factors, whose values are listed in the various panels. One readily sees that the Fermi motion and to some extent the FSI lead to the disappearance of the resonance structure. The ratio of the theoretical cross section to the experimental result is about 1.75, except for $\cos\theta^*_{\pi^0} = -0.9$, where it is about 3. However, the origin of this factor is unclear.

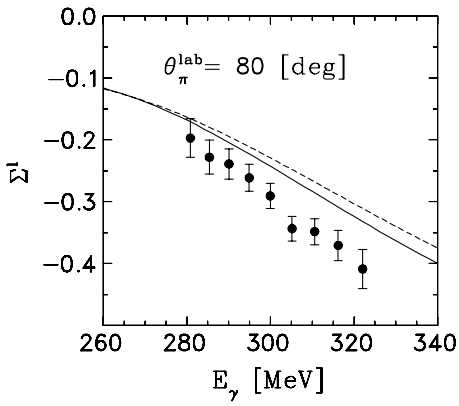

FIG. 25. Linear photon polarization asymmetry for semiexclusive π^- photoproduction on the deuteron at constant pion emission angle $\theta_\pi = 80^\circ$ as a function of photon energy. Notation of curves: dashed, IA; solid, IA + *NN* rescattering. The data are from the LEGS Collaboration (LEGS-exp.L3b) [39].

One possible source could be the neglected interaction of nucleon, resonances with the spectator nucleon, which might result in a broadening of the resonances that is due to additional inelastic processes. In fact, within a simple model calculation for the Δ resonance a significant lowering of the total cross section from such an interaction was found in Ref. [34]. A further source could be the neglected inelasticity of the final *NN* interaction at higher energies. On the other hand, the question arises as to why the same lowering is not observed in the π^- photoproduction in which the agreement with the data is quite satisfactory.

The threshold region is shown in Fig. 20 for π^+ production. Good agreement with the data is achieved, comparable in quality with a recent precision calculation in chiral perturbation theory [36]. The crucial role of the *NN* FSI at low energies, leading to a strong enhancement over the IA, is further demonstrated by the differential cross section with respect to the relative energy of the two final neutrons in π^+ production in Fig. 21 for two different kinematical situations, pion emission in a more forward (left-hand panel) and in a more backward direction (right-hand panel). The $^1S_0$ state of *nn* scattering near threshold, a manifestation of the so-called antibound state as companion to the deuteron, is nicely resolved and also quite well reproduced by the theory if *NN* rescattering is included. A similar result has been reported in Ref. [38].

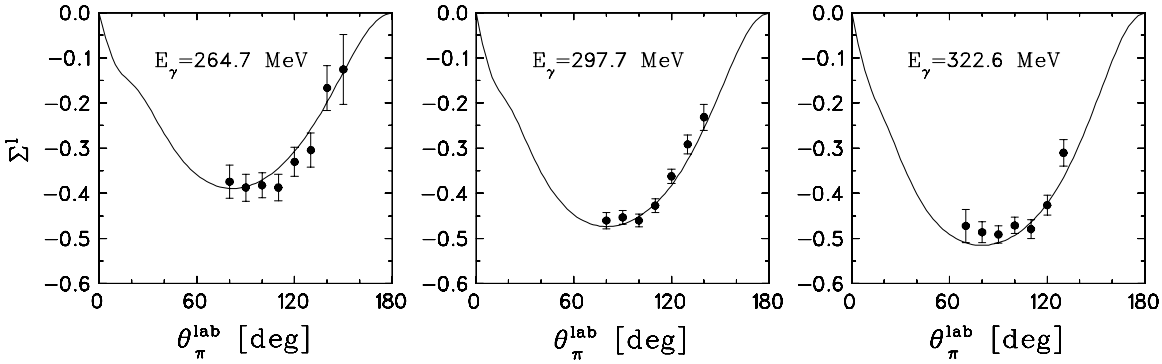

FIG. 26. Linear photon polarization asymmetry for semiexclusive π^0 photoproduction on the deuteron. Solid curves, IA + *NN* rescattering. Experimental data are from the LEGS Collaboration (LEGS-exp.L3b) [39].

With respect to differential cross sections, a comparison for π^- production is exhibited in Fig. 22 and for π^0 production in Fig. 23. For π^- production one notes a satisfactory agreement with experimental data from Benz *et al*. [6], whereas for π^0 production one finds for the three highest energies a slight overestimation of the theory in the maximum and at forward angles an underestimation.

A comparison with data on the unpolarized semiexclusive differential cross section from Benz *et al*. [6] and on Σ^l from the LEGS Collaboration (LEGS-exp.L3b) [39] for π^- production is shown in Fig. 24 for two energies near the Δ region. One notes very little influence from the FSI and quite a good agreement of the theoretical description with the data. Our results on Σ^l are similar to the IA calculation of Lee and Sato [40], but at variance with Ref. [21] in which a larger FSI effect was quoted. However, the latter results are questionable for reasons mentioned above. Another comparison for Σ^l with data from the LEGS Collaboration [39] is exhibited in Fig. 25 for constant pion emission angle as a function of the photon energy. In this case the size is underestimated by the theory, although the FSI shifts the results for the IA in the right direction, but not enough. A much better, almost perfect, agreement with respect to Σ^l is shown in Fig. 26 for π^0 production.

Finally, we show in Fig. 27 for π^- production a comparison between theory and experiment for the semiexclusive differential spin asymmetry $d^2(\sigma^P - \sigma^A)/d\Omega_q$ with respect to circularly polarized photons and the deuteron spin oriented parallel (P) or antiparallel (A) to the photon spin. This spin asymmetry is related to the beam-target asymmetry T_{10}^c according to

$$\frac{d^2(\sigma^P - \sigma^A)}{d\Omega_q} = \sqrt{6}\,\frac{d^2\sigma_0}{d\Omega_q}\,T_{10}^c. \tag{24}$$

Compared with the predictions in Ref. [20] here we find the depth of the minimum at 0° almost independent of the

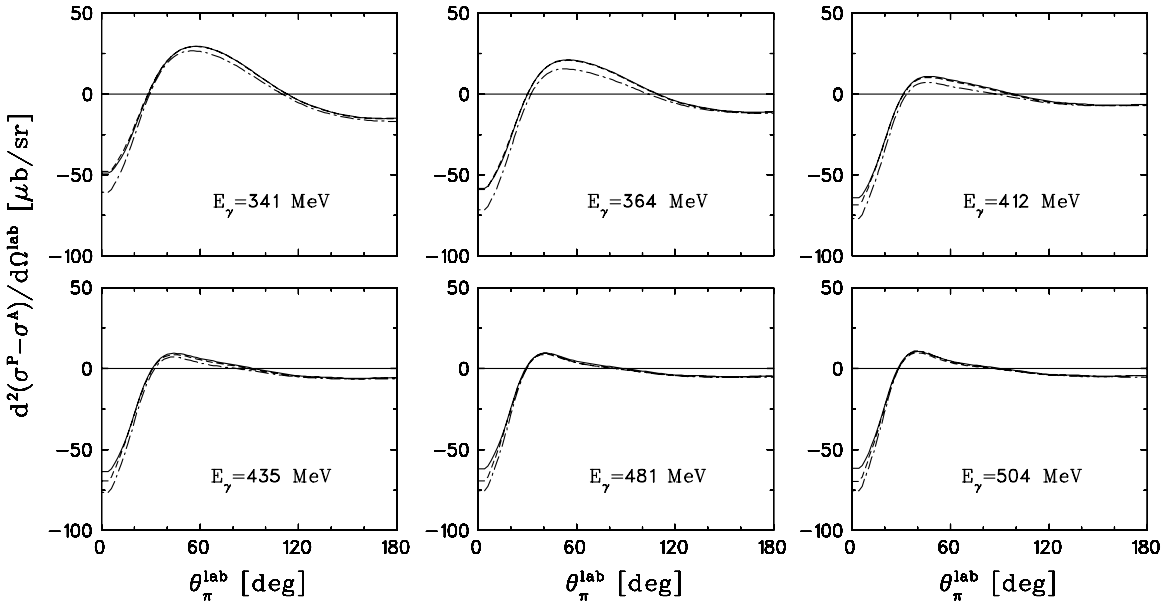

FIG. 27. Circular photon polarization asymmetry for semiexclusive π^- photoproduction on the deuteron. Notation of curves: dashed, IA; solid, IA + *NN* rescattering; dash-dotted, corresponding elementary cross section.

energy and a small positive asymmetry between 30° and 60°. This spin asymmetry has been measured by the A2 Collaboration [41]. However, the analysis of the data is not yet complete. Preliminary data were shown in Ref. [20] without authorization and thus are not shown here. Compared with these, the agreement is quite satisfactory, although in the angular region, where the data are available, the spin asymmetry is very small, almost compatible with zero. Thus it would be very desirable to have additional data at more forward angles, for which the theoretical asymmetry exhibits a pronounced minimum. This concludes the discussion of results.

IV. CONCLUSION AND OUTLOOK

In this work we have explored the role of polarization observables in incoherent pion photoproduction on the deuteron with particular emphasis on the influence of final state interaction in the *NN* and πN subsystems of the final state. In the unpolarized total and semiexclusive differential cross section $d^2\sigma/d\Omega_q$, in which only the direction of the produced pion is measured, the influence of final state rescattering is quite small for charged-pion production for photon energies up to 1 GeV. For π^0 production the influence is much larger. However, the dominant part of the FSI effect arises from the removal of a spurious coherent contribution in the IA when *NN* rescattering is switched on. This is demonstrated by a modified IA, in which the deuteron wave-function component in the final *NN* plane wave is projected out. The remaining FSI effect is comparable with charged-pion production.

As polarization observables we have considered all beam, target, and beam-target asymmetries of the semiexclusive differential cross section. Many of them are quite sizable, in particular the photon asymmetry Σ^l and the various vector asymmetries. The tensor asymmetries are in general considerably smaller. They are often quite insensitive to final state rescattering. Only a few, T_{21}, and T_{21}^c, show a larger influence in charged-pion production.

A very interesting and still open question concerns the disagreement between theoretical and experimental results for $\gamma d \to \pi^0 np$ in the second resonance region. Although our calculation explains the strong smearing of the resonance structure, the data are overestimated by about a factor of 1.5 (see Figs. 18 and 19). It is hoped that new measurements of the ratio

$$R = \frac{d\sigma(\gamma, \pi^0 n)}{d\sigma(\gamma, \pi^0 p)} \tag{25}$$

for quasi-free photoproduction on neutrons and protons can clarify the situation. The old data from Refs. [42,43], pointing to $R = 1$ in the second resonance region, seem to be in disagreement with the results of Ref. [33].

Future theoretical improvements should be devoted to the inclusion of two-body effects in the photoproduction amplitude, e.g., the interaction between a resonance and the spectator nucleon, inclusion of inelasticities in the *NN* interaction, and the role of relativistic effects at higher energies. The problem of off-shell effects for the elementary amplitude is another unsolved task. Furthermore, there is an urgent need for a unified description of single- and double-pion production.

ACKNOWLEDGMENTS

We thank Michael Schwamb for interesting discussions and a careful reading of the manuscript. This work was supported by the Deutsche Forschungsgemeinschaft (SFB 443).

APPENDIX A: SEPARATION OF POLARIZATION ASYMMETRIES

In this appendix we discuss how the various polarization asymmetries of the semi-inclusive differential cross section can be separated by a proper variation of the photon polarization parameters (P_l^γ and P_c^γ), the deuteron polarization parameters (P_1^d and P_2^d), the polarization angles (θ_d and ϕ_d), and the dependence on the pion azimuthal angle ϕ_q, similar to what has been described in [44]. To this end we write the differential cross section of Eq. (9) as follows:

$$\begin{aligned} S\big(P_l^\gamma, P_c^\gamma, P_1^d, P_2^d\big) = S_0\big[1 &+ P_1^d\, A_d^V + P_2^d\, A_d^T \\ &+ P_l^\gamma \left(A_\gamma^l + P_1^d\, A_{\gamma d}^{lV} + P_2^d\, A_{\gamma d}^{lT}\right) \\ &+ P_c^\gamma \left(P_1^d\, A_{\gamma d}^{cV} + P_2^d\, A_{\gamma d}^{cT}\right)\big], \end{aligned} \tag{A1}$$

with $S_0 = S(0, 0, 0, 0)$ as the unpolarized differential cross section. Furthermore, we introduce as generalized single-polarization A asymmetries

$$A_d^V(\theta_q, \phi_{qd}, \theta_d) = \widetilde{T}_{11}^0(\theta_q)\, \sin\phi_{qd}\, d_{10}^1(\theta_d), \tag{A2}$$

$$A_d^T(\theta_q, \phi_q, \phi_{qd}, \theta_d) = \sum_{M=0}^{2} \widetilde{T}_{2M}^0(\theta_q) \cos(M\phi_{qd})\, d_{M0}^2(\theta_d), \tag{A3}$$

$$A_\gamma^l(\theta_q, \phi_q) = \widetilde{\Sigma}^l(\theta_q)\, \cos 2\phi_q, \tag{A4}$$

and double-polarization A asymmetries

$$\begin{aligned} A_{\gamma d}^{lV}(\theta_q, \phi_q, \phi_{qd}, \theta_d) &= \sum_{M=-1}^{1} \widetilde{T}_{1M}^l(\theta_q) \\ &\quad \times \sin(M\phi_{qd} - 2\,\phi_q)\, d_{M0}^1(\theta_d) \\ &= \sum_{M=-1}^{1} \widetilde{T}_{1M}^l(\theta_q)[\sin(M\phi_{qd}) \\ &\quad \times \cos(2\,\phi_q) - \cos(M\phi_{qd}) \\ &\quad \times \sin(2\,\phi_q)]\, d_{M0}^1(\theta_d), \end{aligned} \tag{A5}$$

$$\begin{aligned} A_{\gamma d}^{lT}(\theta_q, \phi_q, \phi_{qd}, \theta_d) &= \sum_{M=-2}^{2} \widetilde{T}_{2M}^l(\theta_q) \\ &\quad \times \cos(M\phi_{qd} - 2\,\phi_q)\, d_{M0}^2(\theta_d) \\ &= \sum_{M=-2}^{2} \widetilde{T}_{2M}^l(\theta_q)[\cos(M\phi_{qd})\, \cos(2\,\phi_q) \\ &\quad + \sin(M\phi_{qd})\, \sin(2\,\phi_q)]\, d_{M0}^2(\theta_d), \end{aligned} \tag{A6}$$

$$A^{cV}_{\gamma d}(\theta_q, \phi_{qd}, \theta_d) = \sum_{M=0}^{1} \widetilde{T}^{c}_{1M}(\theta_q)\, \cos(M\phi_{qd})\, d^{1}_{M0}(\theta_d), \quad \text{(A7)}$$

$$A^{cT}_{\gamma d}(\theta_q, \phi_{qd}, \theta_d) = \sum_{M=1}^{2} \widetilde{T}^{c}_{2M}(\theta_q)\, \sin(M\phi_{qd})\, d^{2}_{M0}(\theta_d). \quad \text{(A8)}$$

Each of these generalized A asymmetries is a function of θ_q and of some of the variables ϕ_q, ϕ_{qd}, and θ_d. The first step is to isolate them by evaluating linear combinations of cross sections for different values of the appropriate polarization parameters $(P^{\gamma}_{l,c}, P^{d}_{1,2})$. For example, A^{l}_{γ} is obtained from the cross-section difference for unpolarized deuterons and linearly polarized photons ($P^{\gamma}_{l} > 0$) minus the unpolarized one ($P^{\gamma}_{l} = 0$), i.e.,

$$A^{l}_{\gamma} = \frac{1}{P^{\gamma}_{l}\, S_0}\left[S\left(P^{\gamma}_{l}, 0, 0, 0\right) - S_0\right]. \quad \text{(A9)}$$

The others can be obtained by the following linear combinations of cross sections:

$$A^{V}_{d} = \frac{1}{2\, P^{d}_{1}\, S_0}\left[S\left(0, 0, P^{d}_{1}, P^{d}_{2}\right) - S\left(0, 0, -P^{d}_{1}, P^{d}_{2}\right)\right], \quad \text{(A10)}$$

$$A^{T}_{d} = \frac{1}{2\, P^{d}_{2}\, S_0}\left[S\left(0, 0, P^{d}_{1}, P^{d}_{2}\right) + S\left(0, 0, -P^{d}_{1}, P^{d}_{2}\right) - 2\, S_0\right], \quad \text{(A11)}$$

$$A^{cV}_{\gamma d} = \frac{1}{4\, P^{\gamma}_{c}\, P^{d}_{1}\, S_0}\left[S\left(0, P^{\gamma}_{c}, P^{d}_{1}, P^{d}_{2}\right) - S\left(0, -P^{\gamma}_{c}, P^{d}_{1}, P^{d}_{2}\right) - S\left(0, P^{\gamma}_{c}, -P^{d}_{1}, P^{d}_{2}\right) + S\left(0, -P^{\gamma}_{c}, -P^{d}_{1}, P^{d}_{2}\right)\right], \quad \text{(A12)}$$

$$A^{cT}_{\gamma d} = \frac{1}{4\, P^{\gamma}_{c}\, P^{d}_{2}\, S_0}\left[S\left(0, P^{\gamma}_{c}, P^{d}_{1}, P^{d}_{2}\right) - S\left(0, -P^{\gamma}_{c}, P^{d}_{1}, P^{d}_{2}\right) + S\left(0, P^{\gamma}_{c}, -P^{d}_{1}, P^{d}_{2}\right) - S\left(0, -P^{\gamma}_{c}, -P^{d}_{1}, P^{d}_{2}\right)\right], \quad \text{(A13)}$$

$$A^{lV}_{\gamma d} = \frac{1}{2\, P^{\gamma}_{l}\, P^{d}_{1}\, S_0}\left[S\left(P^{\gamma}_{l}, 0, P^{d}_{1}, P^{d}_{2}\right) - S\left(0, 0, P^{d}_{1}, P^{d}_{2}\right) - S\left(P^{\gamma}_{l}, 0, -P^{d}_{1}, P^{d}_{2}\right) + S\left(0, 0, -P^{d}_{1}, P^{d}_{2}\right)\right], \quad \text{(A14)}$$

$$A^{lT}_{\gamma d} = \frac{1}{2\, P^{\gamma}_{l}\, P^{d}_{2}\, S_0}\left[S\left(P^{\gamma}_{l}, 0, P^{d}_{1}, P^{d}_{2}\right) - S\left(0, 0, P^{d}_{1}, P^{d}_{2}\right) + S\left(P^{\gamma}_{l}, 0, -P^{d}_{1}, P^{d}_{2}\right) - S\left(0, 0, -P^{d}_{1}, P^{d}_{2}\right) - 2\, P^{\gamma}_{l}\, A^{l}_{\gamma}\, S_0\right]. \quad \text{(A15)}$$

Two of the generalized A asymmetries in Eqs. (A2)–(A8) yield directly one asymmetry each, namely $\widetilde{\Sigma}^{l}$ from A^{l}_{γ} and $\widetilde{T}^{0}_{11}$ from A^{V}_{d}, i.e.,

$$\widetilde{\Sigma}^{l} = A^{l}_{\gamma}(\phi_q = 0), \quad \text{(A16)}$$

$$\widetilde{T}^{0}_{11} = \sqrt{2}\, A^{V}_{d}(\phi_{qd} = \pi/2,\ \theta_d = \pi/2). \quad \text{(A17)}$$

One could also obtain $\widetilde{\Sigma}^{l}$ from taking for linearly polarized photons the cross-section difference of pions in the photon plane to pions perpendicular to this plane, i.e.,

$$\widetilde{\Sigma}^{l} = \frac{1}{P^{\gamma}_{l}} \frac{S\left(P^{\gamma}_{l} > 0, 0, 0, 0\right)|_{\phi_q = 0} - S\left(P^{\gamma}_{l} > 0, 0, 0, 0\right)|_{\phi_q = \pi/2}}{S\left(P^{\gamma}_{l} > 0, 0, 0, 0\right)|_{\phi_q = 0} + S\left(P^{\gamma}_{l} > 0, 0, 0, 0\right)|_{\phi_q = \pi/2}}. \quad \text{(A18)}$$

The remaining general asymmetries A^{T}_{d} and $A^{(l/c)(V/T)}_{\gamma d}$ contain linear combinations of the asymmetries $\widetilde{T}^{0}_{2M}$ and $\widetilde{T}^{l/c}_{\mathrm{IM}}$. To separate the latter, one can exploit the dependence of the A asymmetries on the angular variables ϕ_q, ϕ_{qd}, and θ_d. One achieves this, following the analogous problem in deuteron electrodisintegration [44], by observing that the general functional form of an A asymmetry is

$$A^{I}(\phi_q, \phi_{qd}, \theta_d) = \sum_{M=-I}^{I} \alpha_{\mathrm{IM}}(\phi_q, \phi_{qd}) d^{I}_{M0}(\theta_d), \quad (I = 1, 2), \quad \text{(A19)}$$

where

$$\alpha_{\mathrm{IM}}(\phi_q, \phi_{qd}) = c_{\mathrm{IM}}(\phi_q) \cos M\phi_{qd} + s_{\mathrm{IM}}(\phi_q) \sin M\phi_{qd}\ , \quad \text{(A20)}$$

and the ϕ_q-dependent functions $c_{\mathrm{IM}}(\phi_q)$ and $s_{\mathrm{IM}}(\phi_q)$ have either the form

$$a_0 + a_1 \cos\phi_q + a_2 \cos 2\phi_q \quad \text{(A21a)}$$

or

$$b_1 \sin\phi_q + b_2 \sin 2\phi_q. \quad \text{(A21b)}$$

One should note that for $A^{c(V/T)}_{\gamma d}$, the ϕ_q dependence is absent, i.e., $c_{\mathrm{IM}} \equiv 0$ or $s_{\mathrm{IM}} \equiv 0$, and the sum over M in Eq. (A19) runs from 0 through I. For a given I the M components $\alpha_{\mathrm{IM}}(\phi_q, \phi_{qd})$ of the asymmetry $A^{I}(\phi_q, \phi_{qd}, \theta_d)$ can be separated by a proper choice of θ_d that exploits the properties of the small d^{I}_{M0} functions. For $I = 1$ (vector asymmetries), taking $\theta_d = 0$ or $\pi/2$, i.e., $d^{1}_{M0}(0) = \delta_{M0}$ or $d^{1}_{M0}(\pi/2) = M/\sqrt{2}$, yields α_{10} or α_{11}, respectively, and for the tensor asymmetries ($I = 2$) one may first choose $\theta_d = 0$, yielding with $d^{2}_{M0}(0) = \delta_{M0}$ directly α_{20}. The latter being determined, then by setting $\theta_d = \pi/4$ and $\pi/2$, one can obtain the remaining two terms α_{21} and α_{22}. For the separation of α_{21} and α_{22} one can also choose $\theta_d = \theta^{0}_{d} = \arccos(1/\sqrt{3})$ together with ϕ_{qd} and $\phi_{qd} + \pi$. Then the sum and difference of the corresponding asymmetries result in α_{21} and α_{22}, respectively.

In the next step, to separate the two contributions c_{IM} and s_{IM} in Eq. (A20), one can take first $\phi_{qd} = 0$, giving c_{IM}, and then $\phi_{qd} = \pi/(2M)$ for $M \neq 0$, which yields directly s_{IM}. The remaining separation of the coefficients a_n or b_n in Eqs. (A21) is then achieved by the appropriate choices of ϕ_q. This completes the separation.

APPENDIX B: A MODIFIED IMPULSE APPROXIMATION

For incoherent π^0 photoproduction in the IA, the NN final state is described by a plane wave $|\vec{p}, sm_s\rangle$ that is not

orthogonal to the deuteron wave function. Thus the IA matrix element contains a spurious contribution from coherent π^0 photoproduction, the size of which is governed by the overlap between the plane wave and the deuteron wave function, which is just the deuteron wave function in momentum space [see Eq. (6)]:

$$\phi_{m_s m_d}(\vec{p}\,) = \langle \vec{p}, 1m_s | 1m_d \rangle^{(d)} \neq 0, \tag{B1}$$

whereas, if the interaction between the nucleons is properly taken into account, the overlap with the final *NN*-scattering wave vanishes. Therefore one can expect that a large fraction of *NN*-rescattering effects in incoherent π^0 photoproduction arises from the elimination of the spurious coherent contribution.

One can avoid this spurious contribution by applying a modified IA, in which one uses a modified *NN* final state wave function, in which the deuteron wave-function component is projected out by the replacement:

$$\begin{aligned} |\vec{p}, 1m_s\rangle &\to |\vec{p}, 1m_s\rangle - \sum_{m_d} |1m_d\rangle^{(d)} \langle 1m_d | \vec{p}, 1m_s\rangle \\ &= |\vec{p}, 1m_s\rangle - \sum_{m_d} |1m_d\rangle^{(d)} \phi^*_{m_s m_d}(\vec{p}\,). \end{aligned} \tag{B2}$$

This means the following replacement for the IA matrix element:

$$\begin{aligned} \langle \vec{p}, 1m_s | T | 1m_d \rangle^{(d)} \to \langle \vec{p}, 1m_s | T | 1m_d \rangle^{(d)} \\ - \sum_{m'_d} \phi_{m_s m'_d}(\vec{p}\,)\, {}^{(d)}\langle 1m'_d | T | 1m_d \rangle^{(d)}. \end{aligned} \tag{B3}$$

The matrix element ${}^{(d)}\langle 1m'_d | T | 1m_d \rangle^{(d)}$ corresponds to the one for coherent pion photoproduction $\gamma d \to \pi^0 d$ in the off-shell region. The comparison of the original IA with the modified IA reveals then what fraction of the whole FSI effect arises from the nonorthogonality.

[1] G. F. Chew and H. W. Lewis, Phys. Rev. **84**, 779 (1951).
[2] M. Lax and H. Feshbach, Phys. Rev. **88**, 509 (1952).
[3] I. Blomqvist and J. M. Laget, Nucl. Phys. **A280**, 405 (1977).
[4] J. M. Laget, Nucl. Phys. **A296**, 388 (1978).
[5] J. M. Laget, Phys. Rep. **69**, 1 (1981).
[6] P. Benz *et al.*, Nucl. Phys. **B65**, 158 (1973).
[7] M. I. Levchuk, V. A. Petrun'kin, and M. Schumacher, Z. Phys. A **355**, 317 (1996).
[8] M. I. Levchuk, M. Schumacher, and F. Wissmann, nucl-th/0011041.
[9] R. A. Arndt *et al.*, SAID: available at http://gwdac.phys.gwu.edu/.
[10] D. Drechsel, O. Hanstein, S. S. Kamalov, and L. Tiator, MAID: available at http://www.kph.uni-mainz.de/.
[11] R. Machleidt, K. Holinde, and C. Elster, Phys. Rep. **149**, 1 (1987); R. Machleidt, Adv. Nucl. Phys. **19**, 189 (1989).
[12] M. I. Levchuk, M. Schumacher, and F. Wissmann, Nucl. Phys. **A675**, 621 (2000).
[13] A. Loginov, A. Sidorov, and V. Stibunov, Phys. At. Nucl. **63**, 391 (2000) [Yad. Fiz. **63**, 459 (2000)].
[14] E. M. Darwish, H. Arenhövel, and M. Schwamb, Eur. Phys. J. A **16**, 111 (2003).
[15] E. M. Darwish, H. Arenhövel, and M. Schwamb, Eur. Phys. J. A **17**, 513 (2003).
[16] *Proceedings of the Second International Symposium on the GDH Sum Rule and the Spin Structure of the Nucleon, Genova 2002*, edited by M. Anghinolfi, M. Battaglieri, and R. de Vita (World Scientific, Singapore, 2003); *Proceedings of the Third International Symposium on the GDH Sum Rule and its Extensions, Norfolk, Virginia, 2004*, edited by S. Kuhn and J.-P. Chen (World Scientific, Singapore, 2005).
[17] R. Schmidt, H. Arenhövel, and P. Wilhelm, Z. Phys. A **355**, 421 (1996).
[18] E. M. Darwish, J. Phys. G **31**, 105 (2005).
[19] E. M. Darwish, Nucl. Phys. **A735**, 200 (2004).
[20] E. M. Darwish, Nucl. Phys. **A748**, 596 (2005).
[21] E. M. Darwish, Phys. Lett. **B615**, 61 (2005).
[22] E. M. Darwish and A. Salam, Nucl. Phys. **A759**, 170 (2005).
[23] H. Arenhövel and A. Fix, Phys. Rev. C (accompanying paper CF10004).
[24] H. Arenhövel, A. Fix, and M. Schwamb, Phys. Rev. Lett. **93**, 202301 (2004).
[25] A. Fix and H. Arenhövel, Z. Phys. A **359**, 427 (1997).
[26] J. Haidenbauer and W. Plessas, Phys. Rev. C **30**, 1822 (1984); **32**, 1424 (1985).
[27] S. Nozawa, B. Blankleider, and T.-S. H. Lee, Nucl. Phys. **A513**, 459 (1990).
[28] P. Dennery, Phys. Rev. **124**, 2000 (1961).
[29] A. Salam and H. Arenhövel, Phys. Rev. C **70**, 044008 (2004).
[30] J. Noble, Phys. Lett. **B67**, 39 (1977).
[31] U. Siodlaczek *et al.*, Eur. Phys. J. A **10**,365 (2001).
[32] M. Asai *et al.*, Phys. Rev. C **42**, 837 (1990).
[33] B. Krusche *et al.*, Eur. Phys. J. A **6**, 309 (1999).
[34] C. Reiss, H. Arenhövel, and M. Schwamb, Eur. Phys. J. A **25**, 171 (2005).
[35] E. C. Booth, B. Chasan, J. Comuzzi, and P. Bosted, Phys. Rev. C **20**, 1217 (1979).
[36] V. Lensky, V. Baru, J. Haidenbauer, C. Hanhart, A. E. Kudryavtsev, and U.-G. Meissner, Eur. Phys. J. A **26**, 107 (2005).
[37] G. Köbschall, B. Alberti, H. Jansen, K. Rohrich, C. Schmitt, V. H. Walther, K. Weinand, M. Kobayashi, and H. Arenhövel, Nucl. Phys. **A466**, 612 (1987).
[38] L. Levchuk, L. Canton, and A. Shebeko, Eur. Phys. J. A **21**, 29 (2004).
[39] A. Sandorfi (private communication).
[40] T.-S. H. Lee (private communication).
[41] P. Pedroni (private communication).
[42] C. Bacci *et al.*, Phys. Lett. **B39**, 559 (1972).
[43] Y. Hemmi *et al.*, Nucl. Phys. **B55**, 333 (1975).
[44] H. Arenhövel, W. Leidemann, and E. L. Tomusiak, Eur. Phys. J. A **23**, 147 (2005).